

# BornAgain Developers Reference Physics and Numerics

Work in progress

Last updated June 12, 2023

edited by Joachim Wuttke

Scientific Computing Group  
Jülich Centre for Neutron Science  
at Heinz Maier-Leibnitz Zentrum Garching  
Forschungszentrum Jülich GmbH

For information about BornAgain, see the reference paper Pospelov et al 2020 [1] and the web docs at <https://www.bornagainproject.org>.

This reference provides some of the theory behind the code.

Notation: Bold symbols ( $\mathbf{r}$ ,  $\mathbf{B}$ ) are real or complex 3-vectors. A hat ( $\hat{v}$ ,  $\hat{\sigma}_z$ ) denotes an operator in spin space, represented by a complex  $2 \times 2$  matrix. Spinors are represented by uppercase letters ( $\Psi$ ,  $\Phi$ ,  $T$ ,  $R$ ). Black-board bold ( $\mathbb{M}$ ) denotes  $4 \times 4$  matrices.

Copyright:           Forschungszentrum Jülich GmbH 2013–2023

License:             Creative Commons CC-BY-SA

Editor:              Joachim Wuttke

Authors:            BornAgain developers, see git log  
Scientific Computing Group  
at Heinz Maier-Leibnitz Zentrum (MLZ) Garching

Disclaimer:         Software and documentation are work in progress.  
We cannot guarantee correctness and accuracy.  
If in doubt, contact us for assistance or scientific collaboration.

# Contents

<b>1</b>	<b>Wave propagation and scattering</b>	<b>1:1</b>
1.1	Wave propagation . . . . .	1:1
1.1.1	Neutrons . . . . .	1:1
1.1.2	X-rays . . . . .	1:3
1.1.3	Unified wave equation . . . . .	1:4
1.2	Distorted-wave Born approximation . . . . .	1:4
1.2.1	Distortion versus perturbation . . . . .	1:5
1.2.2	Differential cross section . . . . .	1:6
<b>2</b>	<b>Flat multilayer systems</b>	<b>2:1</b>
2.1	Wave propagation and scattering in layered samples . . . . .	2:1
2.1.1	Wave propagation in 2+1 dimensions . . . . .	2:1
2.1.2	The four DWBA terms . . . . .	2:2
2.1.3	DWBA for layers with constant mean SLD . . . . .	2:3
2.1.4	Wave amplitudes . . . . .	2:5
2.1.5	Modifications for X-rays . . . . .	2:7
2.2	Solution of the split boundary problem . . . . .	2:8
2.2.1	The split boundary problem . . . . .	2:9
2.2.2	Recursive solution . . . . .	2:10
2.3	Implementation . . . . .	2:10
2.3.1	Call chain . . . . .	2:11
2.3.2	Scalar fluxes . . . . .	2:12
<b>3</b>	<b>Scattering by rough interfaces</b>	<b>3:1</b>
3.1	Propagation through graded interfaces . . . . .	3:1
3.1.1	Interface with tanh profile . . . . .	3:1
3.1.2	Névot-Croce factor . . . . .	3:3
3.2	Scattering by a rough interface . . . . .	3:3
3.2.1	Scattering in DWBA . . . . .	3:4
3.2.2	Random potential . . . . .	3:5
3.2.3	Covariance ex machina . . . . .	3:5
3.2.4	Sharp, rough interface . . . . .	3:6
3.2.5	Stepwise reference potential . . . . .	3:7
3.2.6	One-step reference potential . . . . .	3:8
3.2.7	Gaussian roughness . . . . .	3:9

3.2.8	Analytic plane waves approximation . . . . .	3:10
3.2.9	Refracted waves, linearized correlation . . . . .	3:11
3.2.10	Horizontal correlations . . . . .	3:11
3.3	Literature review: reflectivity and scattering from rough surfaces . . . .	3:12
<b>4</b>	<b>Polarized wave propagation and scattering</b>	<b>4:1</b>
4.1	Polarized neutrons in 2+1 dimensions . . . . .	4:1
4.1.1	Schrödinger equation for neutron spinors . . . . .	4:1
4.1.2	Propagation in a multilayer . . . . .	4:2
4.1.3	Wavenumber operator $\hat{\kappa}$ . . . . .	4:2
4.1.4	Eigendecomposition of $\hat{\kappa}$ . . . . .	4:3
4.2	Refraction and reflection at interfaces . . . . .	4:4
4.2.1	Transfer matrix . . . . .	4:5
4.2.2	Phase rotation matrix . . . . .	4:5
4.3	From old document “PolarizedImplementation” . . . . .	4:5
4.3.1	Numerically stable implementation . . . . .	4:6
4.3.2	Roughness . . . . .	4:7
4.3.3	Reflection matrix and boundary conditions . . . . .	4:10
4.3.4	Amplitudes for DWBA computations . . . . .	4:11
4.3.5	Limiting case $\kappa \rightarrow 0$ . . . . .	4:11
4.3.6	Test suite . . . . .	4:12
4.3.7	Magnetic field in BornAgain . . . . .	4:12
4.3.8	Intensity and density matrix . . . . .	4:13
4.4	From old document “Reflectivity” . . . . .	4:15
4.4.1	Parratt formalism . . . . .	4:16
4.5	From old document “Stratified” . . . . .	4:16
4.5.1	The split boundary problem . . . . .	4:17
<b>5</b>	<b>Evanescent waves</b>	<b>5:1</b>
5.1	Vanishing vertical wavenumber, evanescent case etc . . . . .	5:1
5.1.1	Vanishing vertical wavenumber . . . . .	5:1
5.1.2	Opaque layers and evanescent waves . . . . .	5:1
5.1.3	Flux, evanescent waves . . . . .	5:2
<b>6</b>	<b>Instrument simulation</b>	<b>6:1</b>
6.1	Incoming beam and resolution . . . . .	6:1
6.2	Detector images . . . . .	6:1
6.2.1	Pixel coordinates, scattering angles, and $\mathbf{q}$ components . . . . .	6:2
6.2.2	Intensity transformation . . . . .	6:5
	<b>Bibliography</b>	<b>X:1</b>

# 1 Wave propagation and scattering

{SSca}

This chapter introduces the formalism to described neutron and X-ray propagation and scattering, as needed for the analysis of grazing-incidence small-angle scattering (GISAS) experiments.

## 1.1 Wave propagation

{Swave}

In this section, we review the wave equations that describe the propagation of neutrons (Sec. 1.1.1) and X-rays (Sec. 1.1.2) in matter, and combine them into a unified wave equation (Sec. 1.1.3) that is the base for the all following analysis. This provides justification and background for Eqns. 1–3 in the BornAgain reference paper [1].

### 1.1.1 Neutrons

{SnScalar}

The scalar wavefunction  $\psi(\mathbf{r}, t)$  of a free neutron in absence of a magnetic field is governed by the Schrödinger equation

$$i\hbar\partial_t\psi(\mathbf{r}, t) = \left\{ -\frac{\hbar^2}{2m}\nabla^2 + V(\mathbf{r}) \right\} \psi(\mathbf{r}, t). \quad (1.1) \quad \{\text{\texttt{ESchrodi1}}\}$$

Since BornAgain only aims at modelling elastic scattering, any time dependence of the potential is averaged out in the definition  $V(\mathbf{r}) := \langle V(\mathbf{r}, t) \rangle$ . Inelastic scattering, in principle, can be accounted for by an extra contribution damping.<sup>1</sup> Therefore we only need to consider monochromatic waves with given frequency  $\omega$ . In consequence, the wavefunction

$$\psi(\mathbf{r}, t) = \psi(\mathbf{r})e^{-i\omega t} \quad (1.2) \quad \{\text{\texttt{Estationarywave}}\}$$

factorizes into a stationary wave and a time-dependent phase factor. In the following, we will characterize the incoming radiation not by its energy  $\hbar\omega$ , but by its *vacuum wavenumber*  $K$ , given by the dispersion relation

$$\hbar\omega = \frac{(\hbar K)^2}{2m}. \quad (1.3) \quad \{\text{\texttt{Estationarywave}}\}$$

The Schrödinger equation (1.1) then takes the simple form

$$\{\nabla^2 + K^2 - 4\pi v_{\text{nucl}}(\mathbf{r})\} \psi(\mathbf{r}) = 0 \quad (1.4) \quad \{\text{\texttt{EWvEq}}\}$$

<sup>1</sup>This is not explicitly supported in the software, but users are free to increase the imaginary part of the refractive index to emulate damping by inelastic losses.

{Flosses}

with the rescaled form of Fermi's pseudopotential

$$v_{\text{nucl}}(\mathbf{r}) := \frac{m}{2\pi\hbar^2} V(\mathbf{r}) = \sum_j \langle b_j \delta(\mathbf{r} - \mathbf{r}_j(t)) \rangle. \quad (1.5)$$

The sum runs over all nuclei exposed to  $\psi$ . The subscript “nucl” designates nuclear as opposed to magnetic scattering. The *bound scattering length*  $b_j$  is isotope specific; values are tabulated [2].

In *small-angle scattering*, as elsewhere in *neutron optics* [3], the potential can be coarse-grained by spatially averaging over at least a few atomic diameters,

$$v_{\text{nucl}}(\mathbf{r}) = \sum_s b_s \rho_s(\mathbf{r}), \quad (1.6)$$

where the sum now runs over chemical elements,  $b_s := \langle b_j \rangle_{j \in s}$  is the bound *coherent* scattering length, and  $\rho_s$  is a number density. In passing from (1.5) to (1.6), we neglected *Bragg scattering* from atomic-scale correlation, and *incoherent scattering* from spin or isotope related fluctuations of  $b_j$ . In small-angle experiments, these types of scattering only matter as loss channels.<sup>2</sup> Furthermore, incoherent scattering, as inelastic scattering, contributes to the diffuse background in the detector. In conclusion, the coarse-grained neutron optical potential (1.6) is just a *scattering length density* (SLD) [3, eq. 2.8.37].

In general, the incident neutron beam in a scattering experiment is not a *pure* quantum state, but a statistical mixture of such states, and must therefore be described by a density matrix,

$$\hat{\rho} := \sum_j p_j |\psi_j\rangle \langle \psi_j|, \quad (1.7) \quad \{\{\text{EdefRho}}\}$$

where  $p_j$  is the probability of pure state  $\psi_j$ . Let us define the wave vector operator  $\hat{\mathbf{k}}$  and the flux operator

$$\hat{\mathbf{J}} := |\mathbf{r}\rangle \langle \mathbf{r}| \hat{\mathbf{k}} + \hat{\mathbf{k}}^\dagger |\mathbf{r}\rangle \langle \mathbf{r}|. \quad (1.8) \quad \{\{\text{EdefJop}}\}$$

The current density, or *flux*, is then given by

$$\mathbf{J}(\mathbf{r}) := \text{Tr}\{\hat{\rho}\hat{\mathbf{J}}\} \propto \sum_j p_j \left\{ \psi_j(\mathbf{r})^* \frac{\nabla}{2i} \psi_j(\mathbf{r}) - \psi_j(\mathbf{r}) \frac{\nabla}{2i} \psi_j(\mathbf{r})^* \right\}. \quad (1.9) \quad \{\{\text{EdefJ}}\}$$

This is in arbitrary units, since we do not impose a specific normalization on the unbound wavefunction  $\psi$ . To compute scattering cross sections, we will only need the *ratio* of scattered to incident flux. Mostly we will assume pure states to be *plane waves*

$$\psi_{\mathbf{k}}(\mathbf{r}) := e^{i\mathbf{k}\mathbf{r}}. \quad (1.10) \quad \{\{\text{EplaneWave}}\}$$

In vacuum, the wavevector  $\mathbf{k}$  purely real. We replace the sum in (1.7) by an integral, and find that the flux is simply

$$\mathbf{J}(\mathbf{r}) = \int d^3k p_{\mathbf{k}} |\psi_{\mathbf{k}}(\mathbf{r})|^2 \mathbf{k}. \quad (1.11) \quad \{\{\text{EplaneWave}}\}$$

<sup>2</sup>Same remark as in Footnote 1: To model these losses, use the imaginary part of the refractive index.



For stationary oscillations (1.13), the time average is

$$\langle \mathbf{S} \rangle = \frac{1}{4} \langle \mathbf{E}(\mathbf{r}) \times \mathbf{H}(\mathbf{r})^* + \text{c. c.} \rangle. \quad (1.19)$$

We specialize to vacuum with  $\epsilon(\mathbf{r}) = 1$ , and obtain

$$\langle \mathbf{S} \rangle = \frac{1}{4i\omega\mu_0} (\mathbf{E}^*(\mathbf{r}) \times (\nabla \times \mathbf{E}(\mathbf{r})) + \text{c. c.}). \quad (1.20)$$

For a plane wave  $\mathbf{E}(\mathbf{r}) = \mathbf{E}_{\mathbf{k}} e^{i\mathbf{k}\mathbf{r}}$ , we find

$$\langle \mathbf{S} \rangle = \frac{1}{2\omega\mu_0} |\mathbf{E}_{\mathbf{k}}|^2 \text{Re } \mathbf{k}, \quad (1.21)$$

which confirms the common knowledge that the radiation intensity counted in a detector is proportional to the squared electric field amplitude.

### 1.1.3 Unified wave equation

As in Eqns. 1–3 of Ref. [1], we combine all the above in a unified wave equation

{SuniWave}

$$(D_0 - 4\pi v(\mathbf{r})) \psi(\mathbf{r}) = 0 \quad (1.22) \quad \{\text{EWAVE}\}$$

with the vacuum wave operator

$$D_0 := \begin{cases} \nabla^2 + K^2 & \text{for neutrons,} \\ \nabla^2 - \nabla \cdot \nabla + K^2 & \text{for X-rays} \end{cases} \quad (1.23) \quad \{\text{EDo}\}$$

and the potential<sup>5</sup>

$$v(\mathbf{r}) := \begin{cases} v_{\text{nucl}}(\mathbf{r}) & \text{for neutrons,} \\ K^2(1 - \epsilon(\mathbf{r}))/4\pi & \text{for X-rays.} \end{cases} \quad (1.24) \quad \{\text{ETV}\}$$

The generic wave amplitude  $\psi$  shall represent the scalar neutron wavefunction  $\psi$  or the electric field  $\mathbf{E}$ .

---

<sup>5</sup>This corrects Eq. 3 in our reference paper [1], which had a sign error in the X-ray case.



{SDWBA}

{Sdecompose}

{{Edecompose}}

{{EDPsi}}

{EDPsi}

{{EDPsi0}}

{{EnkK}}

## 1.2 Distorted-wave Born approximation

Neutron or X-ray scattering by condensed matter is usually described in *Born approximation* (BA), which treats the whole potential  $v(\mathbf{r})$  as a small perturbation. This is not adequate if incident or scattered wave propagate under small grazing angles, as refraction and reflection are no longer small. For grazing-incidence small-angle scattering, we need the more generic *distorted-wave Born approximation* (DWBA).<sup>6</sup>

### 1.2.1 Distortion versus perturbation

To get started, we decompose the potential (1.24) into a more *regular* and a more *fluctuating* part:

$$v(\mathbf{r}) =: \bar{v}(\mathbf{r}) + \delta v(\mathbf{r}). \quad (1.25)$$

The *distortion field*  $\bar{v}$  comprises regular, well-known features of the sample. The *perturbation potential*  $\delta v$  stands for the more irregular, unknown features of the sample one ultimately wants to study in a scattering experiment. The wave equation (1.22) shall henceforth be written as

$$(D(\mathbf{r}) - 4\pi\delta v(\mathbf{r}))\psi(\mathbf{r}) = 0 \quad (1.26)$$

with the *distorted wave operator*

$$D(\mathbf{r}) := D_0 - 4\pi\bar{v}(\mathbf{r}). \quad (1.27)$$

Only  $\delta v$  shall be treated as a perturbation. The propagation of incident and scattered waves under the influence of  $\bar{v}$ , in contrast, shall be handled exactly, through analytical solution of the *unperturbed distorted wave equation*

$$D(\mathbf{r})\psi(\mathbf{r}) = 0. \quad (1.28)$$

The solutions are called *distorted* because they differ from the plane waves obtained in the vacuum case  $\bar{v} = 0$ .

Except for neutrons in a magnetic field the distortion field is scalar so that it can be expressed through the *refractive index*

$$n(\mathbf{r}) := \sqrt{1 - \frac{4\pi\bar{v}(\mathbf{r})}{K^2}} = \begin{cases} \sqrt{1 - 4\pi\bar{v}_{\text{nucl}}(\mathbf{r})/K^2} & \text{for neutrons,} \\ \sqrt{\epsilon(\mathbf{r})} & \text{for X-rays.} \end{cases} \quad (1.29)$$

<sup>6</sup>The DWBA was originally devised by Massey and Mott (ca 1933) for collisions of charged particles. Summaries can be found in some quantum mechanics textbooks (Messiah, Schiff) and in monographs on scattering theory (e. g. Newton). The first explicit applications to grazing-incidence scattering were published in 1982: Vineyard [6] discussed X-ray scattering, but failed to account for the distortion of the scattered wave; Mazur and Mills [7] deployed heavy formalism to compute the inelastic neutron scattering cross section of ferromagnetic surface spin waves from scratch. A concise derivation of the DWBA cross section was provided by Dietrich and Wagner (1984/85) for X-rays [8] and neutrons [9]. Unfortunately, their work was overlooked in much of the later literature, which often fell back to less convincing derivations.

If  $\bar{v}(\mathbf{r})$  or  $\epsilon(\mathbf{r})$  has an imaginary part, describing absorption, then  $n(\mathbf{r})$  is a complex number. Conventionally,  $n$  is parameterized by two real numbers:

$$n =: 1 - \delta + i\beta. \quad (1.30) \quad \{\text{\texttt{Endb1}}\}$$

For thermal neutrons and X-rays,  $\delta$  and  $\beta$  are almost always nonnegative,<sup>7</sup> and much smaller than 1. This explains why in most scattering geometries the ordinary Born approximation with  $\bar{v} \equiv 0$  is perfectly adequate. In layered samples under grazing incidence, however, even small differences in  $n$  can cause substantial *refraction* and *reflection*. To model GISAS, therefore, it is necessary to use DWBA with  $\bar{v}(z)$  given by the horizontally averaged refractive index  $\bar{n}(z)$ .

## 1.2.2 Differential cross section

\{\text{\texttt{SdiffCross}}\}

The ratio of the scattered flux  $J(\mathbf{r})$  hitting an infinitesimal detector area  $r^2 d\Omega$  to the incident flux  $J_i$  is expressed as a *differential cross section*

$$\frac{d\sigma}{d\Omega} := \frac{r^2 J(\mathbf{r})}{J_i}. \quad (1.31) \quad \{\text{\texttt{Exsectiondef}}\}$$

The geometric factors that are needed to convert  $d\sigma/d\Omega$  into detector counts will be discussed below in Sec. 6.2.

From standard textbooks we take the generic differential cross section of elastic scattering in first order Born approximation,<sup>8</sup>

$$\frac{d\sigma}{d\Omega} = |\langle \psi_i | \delta v | \psi_f \rangle|^2, \quad (1.32) \quad \{\text{\texttt{Exsection}}\}$$

where the matrix element in Dirac bra-ket notation stands for the integral

$$\langle \psi_i | \delta v | \psi_f \rangle := \int d^3r \psi_i^*(\mathbf{r}) \delta v(\mathbf{r}) \psi_f(\mathbf{r}). \quad (1.33) \quad \{\text{\texttt{Etrama}}\}$$

For brevity and mathematical convenience, the integral has no bounds and therefore formally runs over the entire space. However,  $\delta v(\mathbf{r})$  is nonzero only if  $\mathbf{r}$  lies inside the finite sample volume.

In ordinary (non-distorted) Born approximation, the incident  $\psi_i$  is a plane wave (1.10). By means of a far-field expansion, the outgoing spherical wave  $\psi_f$ , traced back from the detector towards the sample, is also approximated as a plane wave. Thereby (1.33) becomes a Fourier integral

$$\langle \psi_i | \delta v | \psi_f \rangle = \int d^3r e^{-i\mathbf{k}_i \mathbf{r}} \delta v(\mathbf{r}) e^{i\mathbf{k}_f \mathbf{r}} = \int d^3r e^{i\mathbf{q} \mathbf{r}} \delta v(\mathbf{r}) \quad (1.34) \quad \{\text{\texttt{Etramaq}}\}$$

with the scattering vector

$$\mathbf{q} := \mathbf{k}_f - \mathbf{k}_i. \quad (1.35) \quad \{\text{\texttt{Etramaq}}\}$$

<sup>7</sup>The plus sign in front of  $i\beta$  is a consequence of the quantum-mechanical sign convention; in the X-ray crystallography convention it would be a minus sign.

<sup>8</sup>For a particularly detailed derivation see Schober's lecture notes on neutron scattering [10].

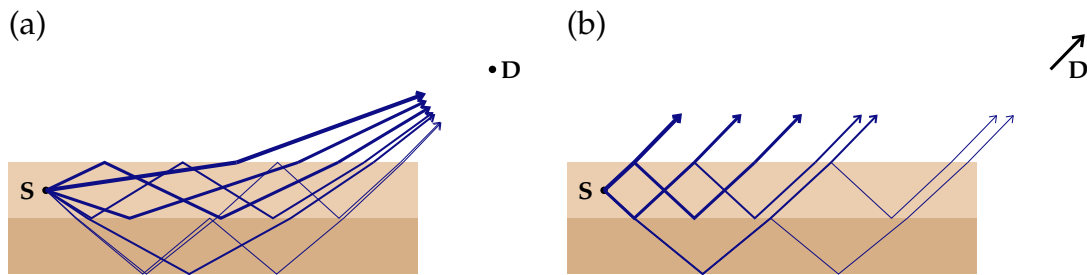


Figure 1.1: (a) In a multilayer sample, the scattered wave propagates from the scattering center  $S$  towards the detector  $D$  through different paths, due to partial reflection by interfaces. (b) In far-field approximation, the detector location is so remote that all rays leaving the sample can be considered parallel. In consequence, when the scattered wave is traced back from the detector it can be considered plane until it reaches the sample.

{Fgreen1}

This plane-wave approximation breaks down under grazing incidence as refraction and reflection by surfaces and interfaces cannot be neglected. While (1.32) and (1.33) still hold, (1.34) does not. In DWBA, the incident wave  $\psi_i$  ceases to be plane when it reaches the sample (Fig. 1.1). Inside the sample it evolves according to the unperturbed wave equation (1.28). Similarly, the scattered wave  $\psi_f$ , traced back from the detector, is a plane wave outside the sample, but is distorted inside the sample as it obeys (1.28). The wave propagation inside a discrete multilayer sample will be worked out in Chapter 2.

## 2 Flat multilayer systems

{sec:Multilayers}

This chapter specializes the DWBA for a multilayer system with  $\bar{v}(\mathbf{r}) = \bar{v}(z)$ .

### 2.1 Wave propagation and scattering in layered samples

{Swave21}

#### 2.1.1 Wave propagation in 2+1 dimensions

{Sgrazingwave}

We now specialize the results from Chapter 1 to wave propagation in a sample that is, on average, translationally invariant in 2 dimensions. Following standard convention, we choose the surface of the sample in the  $xy$  plane, and its normal along  $z$ . In visualizations, we will always represent the  $xy$  plane as *horizontal*, and the  $z$  axis as upward *vertical*, although there are “horizontal” reflectometers where the sample is upright to allow for a horizontal scattering plane.

Scattering from such systems will be studied in distorted-wave Born approximation. To determine the neutron scattering cross section (1.32), we need to determine the incident and final wavefunctions  $\psi_i$  and  $\psi_f$ . Vertical variations of the refractive index  $n(z)$  cause refraction and reflection. For waves propagating at small glancing angles, the reflectance can take any value between 0 and 1, even though  $1 - n$  is only of the order  $10^{-5}$  or smaller. Such zeroth-order effects cannot be accounted for by perturbative scattering theory. Instead, we need to deal with refraction and reflection from the onset, in the wave propagation equation. Accordingly, the SLD decomposition (1.25) takes the form

$$v(\mathbf{r}) = \bar{v}(z) + \delta v(\mathbf{r}), \quad (2.1) \quad \{\{Edecompose\_z\}\}$$

and the unperturbed distorted wave equation (1.28) becomes

$$\{\nabla^2 + k(z)^2\} \psi(\mathbf{r}) = 0. \quad (2.2) \quad \{\{EWaveZ\}\}$$

Below and above the sample,  $k(z) = \text{const}$ : in these regions,  $\psi(\mathbf{r})$  is a superposition of plane waves. The exciting wavefunction is

$$\psi_e(\mathbf{r}) = e^{i\mathbf{k}_{\parallel}\mathbf{r}_{\parallel} + ik_{\perp}z}, \quad (2.3) \quad \{\{Epsiminus\}\}$$

The subscripts  $\parallel$  and  $\perp$  refer to the sample  $xy$  plane. The wavevector components  $\mathbf{k}_{\parallel}$  and  $k_{\perp}$  must fulfill

$$k(z)^2 = \mathbf{k}_{\parallel}^2 + k_{\perp}^2. \quad (2.4) \quad \{\{Epsiminus\}\}$$

Continuity across the sample implies

$$\mathbf{k}_{\parallel} = \text{const.} \quad (2.5) \quad \{\{\text{Ekconst}\}\}$$

From here on, we abbreviate

$$\kappa := k_{\perp}. \quad (2.6) \quad \{\{\text{Dkappa}\}\}$$

When the incident wave hits the sample, it is wholly or partly reflected. Therefore, the full the solution of (2.2) in the half space of the radiation source is

$$\psi(\mathbf{r}) = e^{i\mathbf{k}_{\parallel}\mathbf{r}_{\parallel} + i\kappa_e z} + R e^{i\mathbf{k}_{\parallel}\mathbf{r}_{\parallel} - i\kappa_e z} \quad (2.7) \quad \{\{\text{Eref1}\}\}$$

with a complex reflection coefficient  $R$ . The reflected flux is given by the reflectance  $|R|^2$ . In the opposite halfspace, the solution of (2.2) is simply

$$\psi(\mathbf{r}) = T e^{i\mathbf{k}_{\parallel}\mathbf{r}_{\parallel} + i\kappa_e z} \quad (2.8) \quad \{\{\text{Etra1}\}\}$$

with a complex transmission coefficient  $T$ . The transmitted flux is given by the transmittance  $|T|^2$ . As before, subscript e stands for the exciting wave in vacuum outside the sample.

Within the sample, the wave equation (2.2) is solved by the factorization ansatz

$$\psi(\mathbf{r}) = e^{i\mathbf{k}_{\parallel}\mathbf{r}_{\parallel}} \phi(z). \quad (2.9) \quad \{\{\text{Ekpar}\}\}$$

The vertical wavefunction  $\phi(z)$  is governed by the one-dimensional wave equation

$$\left\{ \partial_z^2 + k(z)^2 - k_{\parallel}^2 \right\} \phi(z) = 0. \quad (2.10) \quad \{\{\text{Ewavez}\}\}$$

As solution of a differential equation of second degree,  $\phi(z)$  can be written as superposition of a downward travelling wave  $\phi^-(z)$  and an upward travelling wave  $\phi^+(z)$ . Accordingly, the three-dimensional wavefunction can be written as

$$\psi(\mathbf{r}) = \psi^-(\mathbf{r}) + \psi^+(\mathbf{r}). \quad (2.11) \quad \{\{\text{Epsisumpm}\}\}$$

## 2.1.2 The four DWBA terms

All the above holds not only for the incident wavefunction  $\psi_i$ , but also for the wavefunction  $\psi_f$  that is tracked back from a detector pixel towards the sample. Therefore the scattering matrix element involves two incident and two final partial wavefunctions. The resulting sum

$$\langle \psi_i | \delta v | \psi_f \rangle = \langle \psi_i^- | \delta v | \psi_f^- \rangle + \langle \psi_i^- | \delta v | \psi_f^+ \rangle + \langle \psi_i^+ | \delta v | \psi_f^- \rangle + \langle \psi_i^+ | \delta v | \psi_f^+ \rangle \quad (2.12) \quad \{\{\text{Edwba4}\}\}$$

is depicted in Figure 2.1. It can be written in an obvious shorthand notation

$$\langle \psi_i | \delta v | \psi_f \rangle = \sum_{\pm_i} \sum_{\pm_f} \langle \psi_i^{\pm} | \delta v | \psi_f^{\pm} \rangle. \quad (2.13) \quad \{\{\text{Edwba}\}\}$$

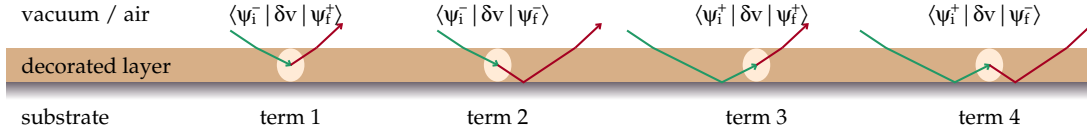


Figure 2.1: The four terms in the DWBA scattering matrix element (2.13). Note that this is a highly simplified visualization. In particular, it does not show multiple reflections of incoming or scattered radiation, though they are properly accounted for by DWBA theory and by all simulation software.

{Fdwba4terms}

This equation contains the essence of the DWBA for GISAS, and is the base for all scattering models implemented in BornAgain. Since  $\langle \psi_i | \delta v | \psi_f \rangle$  appears as a squared modulus in the differential cross section (1.32), the four terms of (2.13) can interfere with each other, which adds to the complexity of GISAS patterns.

BornAgain supports multilayer samples with refractive index discontinuities at layer interfaces. Conventions for layer numbers and interface coordinates are introduced in Figure 2.2. A sample has  $N$  layers, including the semi-infinite bottom and top layers. Numbering is from top to bottom, and from 0 to  $N - 1$  as imposed by the programming languages C++ and Python. Each layer  $l$  has a constant refractive index  $n_l$  and a constant wavenumber  $k_l := K_{\text{vac}} n_l$ . Any up- or downward travelling solution of the wave equation shall be written as a sum over partial wavefunctions,

$$\psi^\pm(\mathbf{r}) = \sum_l \psi_l^\pm(\mathbf{r}), \quad (2.14) \quad \{\{\text{Epsipmsuml}\}\}$$

with the requirement

$$\psi_l^\pm(\mathbf{r}) = 0 \text{ for } \mathbf{r} \text{ outside layer } l. \quad (2.15) \quad \{\{\text{Epsipmloutside}\}\}$$

The DWBA matrix element (2.13) then takes the form

$$\langle \psi_i | \delta v | \psi_f \rangle = \sum_l \sum_{\pm_i} \sum_{\pm_f} \langle \psi_{i,l}^\pm | \delta v | \psi_{f,l}^\pm \rangle. \quad (2.16) \quad \{\{\text{Edwbal}\}\}$$

### 2.1.3 DWBA for layers with constant mean SLD

{SSStep}

We now specialize to the case that  $\bar{v}(z)$  is a step function: within each layer,  $\bar{v}(z) =: v_l$  is constant. Accordingly, within the layer, the directional neutron wavefunction  $\psi_l^\pm$  is a plane wave and factorizes as in (2.9). Its amplitude  $A_l^\pm$  is determined recursively by Fresnel's transmission and reflection coefficients that are based on continuity conditions at the layer interfaces. This will be elaborated in Section 2.1.4. The vertical wavenumber is determined by (2.3) and (2.5),

$$\kappa_l^\pm = \pm \sqrt{k_l^2 - k_\parallel^2}. \quad (2.17) \quad \{\{\text{Ekperp1}\}\}$$

In the absence of absorption and above the critical angle, wavevectors are real so that we can describe the beam in terms of a glancing angle

$$\alpha_l := \arctan(\kappa_l / k_\parallel). \quad (2.18) \quad \{\{\text{Edef\_alpha}\}\}$$

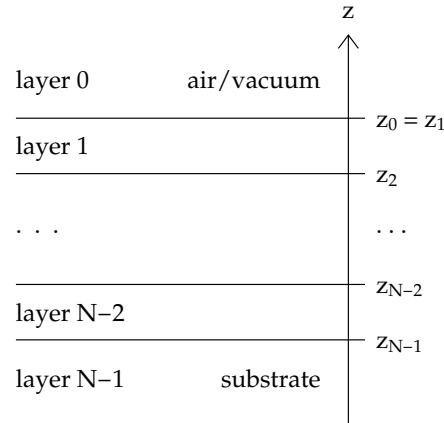


Figure 2.2: Conventions for layer numbers and interface coordinates. A sample has  $N$  layers, including the semi-infinite bottom and top layers. Layers are numbered from top to bottom. The top vacuum (or air) layer (which extends to  $z \rightarrow +\infty$ ) has number 0, the substrate (extending to  $z \rightarrow -\infty$ ) is layer  $N - 1$ . The parameter  $z_l$  is the  $z$  coordinate of the *top* interface of layer  $l$ , except for  $z_0$  which is the coordinate of the *bottom* interface of the air or vacuum layer 0.

{Fdefz}

Equivalently,

$$k_{\parallel} = K n_l \cos \alpha_l. \quad (2.19) \quad \{\{Ekplllncos\}\}$$

Since  $k_{\parallel}$  is constant across layers, we have

$$n_l \cos \alpha_l = \text{the same for all } l, \quad (2.20) \quad \{\{ESnell\}\}$$

which is Snell's refraction law. In general, however, the vertical wavenumber  $\kappa_l$ , determined by  $k_l$  and  $k_{\parallel}$  as per (2.3), can become imaginary (total reflection conditions) or complex (absorbing layer). In these cases, glancing angles are no longer well defined, and the geometric interpretation of  $\psi_l(\mathbf{r})$  less obvious. so that one has to fully rely on the algebraic formalism.

With the indicator function

$$\chi_l(\mathbf{r}) := \begin{cases} 1 & \text{if } z_l \leq z \leq z_{l+1}, \\ 0 & \text{otherwise,} \end{cases} \quad (2.21) \quad \{\{Echildef\}\}$$

the vertical wavefunction can be written

$$\phi_l^{\pm}(z) = A_l^{\pm} e^{\pm i \kappa_l (z - z_l)} \chi_l(z). \quad (2.22) \quad \{\{Ephizwj\}\}$$

The offset  $z_l$  has been included in the phase factor for later convenience. See Sec. 5.1.1 for the case of vanishing  $\kappa$ .

The DWBA transition matrix element (2.13) is

$$\langle \psi_i | \delta v | \psi_f \rangle = \sum_l \sum_{\pm_i} \sum_{\pm_f} A_{il}^{\pm_i*} A_{fl}^{\pm_f} \delta v_l(\mathbf{k}_{fl}^{\pm_f} - \mathbf{k}_{il}^{\pm_i}) \quad (2.23) \quad \{\{Edwba_m10\}\}$$

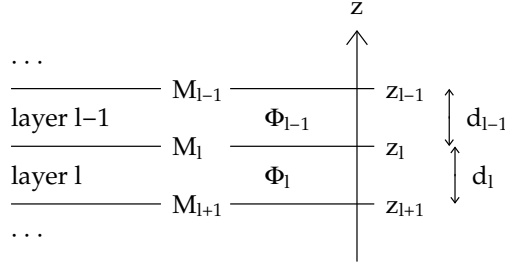


Figure 2.3: The transfer matrix  $M_l$  connects the wavefunctions  $\Phi_l, \Phi_{l-1}$  in adjacent layers. {Fboundary}

with the Fourier transform of the SLD restricted to layer  $l$

$$\delta v_l(\mathbf{q}) := \int_{z_l}^{z_{l+1}} dz \int d^2 r_{\parallel} e^{i\mathbf{q}\mathbf{r}} \delta v(\mathbf{r}) = \int d^3 r e^{i\mathbf{q}\mathbf{r}} \delta v(\mathbf{r}) \chi_l(z). \quad (2.24) \quad \{\text{Echi j}\}$$

To alleviate later calculations, we number the four DWBA terms from 1 to 4 as shown in Fig. 2.1, and define the corresponding wavenumbers and amplitude factors and as

$$\begin{aligned} \mathbf{q}^1 &:= \mathbf{k}_f^+ - \mathbf{k}_i^-, & C^1 &:= A_i^{-*} A_f^+, \\ \mathbf{q}^2 &:= \mathbf{k}_f^- - \mathbf{k}_i^-, & C^2 &:= A_i^{-*} A_f^-, \\ \mathbf{q}^3 &:= \mathbf{k}_f^+ - \mathbf{k}_i^+, & C^3 &:= A_i^{+*} A_f^+, \\ \mathbf{q}^4 &:= \mathbf{k}_f^- - \mathbf{k}_i^+, & C^4 &:= A_i^{+*} A_f^-. \end{aligned} \quad (2.25) \quad \{\text{Eundef}\}$$

Accordingly, we can write (2.23) as

$$\langle \psi_i | \delta v | \psi_f \rangle = \sum_l \sum_u C_l^u \delta v_l(\mathbf{q}_l^u). \quad (2.26) \quad \{\text{Edwba\_ml}\}$$

Since  $\mathbf{k}_{\parallel} = \text{const}$ , all wavevectors  $\mathbf{q}_l^u$  have the same horizontal component  $\mathbf{q}_{\parallel}$ ; they differ only in their vertical component  $q_{l\perp}^u$ .

### 2.1.4 Wave amplitudes {Sacrolay}

The plane-wave amplitudes  $A_{wl}^{\pm}$  need to be computed recursively from layer to layer. Since these computations are identical for incident and final waves, we omit the subscript  $w$  in the remainder of this section. At layer interfaces, the optical potential changes discontinuously. From elementary quantum mechanics we know that piecewise solutions of the Schrödinger equations must be connected such that the wavefunction  $\phi(\mathbf{r})$  and its first derivative  $\nabla \phi(\mathbf{r})$  evolve continuously.

To deal with the coordinate offsets introduced in (2.22), we introduce the function

$$d_l := z_l - z_{l+1}, \quad (2.27) \quad \{\text{Edldef}\}$$

which is the thickness of layer  $l$ , except for  $l = 0$ , where the special definition of  $z_0$  (Fig. 2.2) implies  $d_0 = 0$ . We consider the interface between layers  $l$  and  $l - 1$ ,



with  $l = 1, \dots, N - 1$ , as shown in Fig. 2.3. This interface has the vertical coordinate  $z_l = z_{l-1} - d_{l-1}$ . Accordingly, the continuity conditions at the interface are

$$\begin{aligned}\phi_l(z_l) &= \phi_{l-1}(z_{l-1} - d_{l-1}), \\ \partial_z \phi_l(z_l) &= \partial_z \phi_{l-1}(z_{l-1} - d_{l-1}).\end{aligned}\tag{2.28} \quad \{\text{Econtcond}\}$$

We define the phase factor

$$\delta_l := e^{i\kappa_l d_l}.\tag{2.29} \quad \{\text{Ddel1}\}$$

Here and in the following, we will write the downward travelling transmitted and of the upward travelling reflected amplitude as

$$t_l := A_l^- \quad \text{and} \quad r_l := A_l^+.\tag{2.30} \quad \{\text{Ddel1}\}$$

For the plane waves (2.22), the continuity conditions (2.28) take the form

$$\begin{aligned}t_l + r_l &= \delta_{l-1} t_{l-1} + \delta_{l-1}^{-1} r_{l-1}, \\ -\kappa_l t_l + \kappa_l r_l &= -\kappa_{l-1} \delta_{l-1} t_{l-1} + \kappa_{l-1} \delta_{l-1}^{-1} r_{l-1}.\end{aligned}\tag{2.31} \quad \{\text{Econt2}\}$$

After some lines of linear algebra, we can rewrite this equation system as

$$\begin{pmatrix} t_{l-1} \\ r_{l-1} \end{pmatrix} = M_l \begin{pmatrix} t_l \\ r_l \end{pmatrix}\tag{2.32} \quad \{\text{EcMc}\}$$

with the transfer matrix<sup>1</sup>

$$M_l := \Delta_{l-1} S_l,\tag{2.33} \quad \{\text{EMil}\}$$

which we write using the phase rotation matrix

$$\Delta_l := \begin{pmatrix} \delta_l^{-1} & 0 \\ 0 & \delta_l \end{pmatrix}\tag{2.34} \quad \{\text{DmatD}\}$$

and the refraction matrix

$$S_l := \frac{1}{2} \begin{pmatrix} s_l^+ & s_l^- \\ s_l^- & s_l^+ \end{pmatrix}\tag{2.35} \quad \{\text{DmatS}\}$$

with coefficients

$$s_l^\pm := 1 \pm \kappa_l / \kappa_{l-1}.\tag{2.36} \quad \{\text{Ds1pm}\}$$

Energy conservation can be easily verified for real-valued wave numbers. The vertical flux is  $J = |\Phi|^2 \kappa$ . Under the action of either  $\Delta$  or  $S$ ,

$$\kappa_l (|t_l|^2 - |r_l|^2) = \text{const for all } l.\tag{2.37} \quad \{\text{EConservation}\}$$

---

<sup>1</sup>This approach is generally attributed to Abelès, who elaborated it in his thesis from 1949, published 1950. The usually cited paper [11] is no more than a short advertisement.

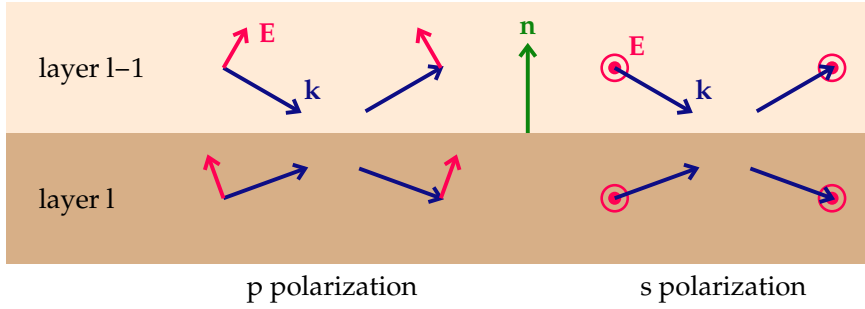


Figure 2.4: Conventions for polarization directions relative to a refracting interface: For  $p$  polarization, the electric field vector  $\mathbf{E}$  is parallel to the interface normal  $\mathbf{n}$ ; for  $s$  polarization, it is perpendicular (*senkrecht* in German). In either case,  $\mathbf{E}$  is perpendicular to the wavevector  $\mathbf{k}$ .

{Fsppol}

### 2.1.5 Modifications for X-rays

{SmulayX}

We shall now translate the above results from unpolarized neutrons to X-rays. The vectorial amplitude of the electromagnetic field will require nontrivial modifications. In place of the factorization (2.9), we write

$$\mathbf{E}(\mathbf{r}) = e^{i\mathbf{k}_{\parallel}\mathbf{r}}\Phi(z). \quad (2.38) \quad \text{{EConservation}}$$

In place of (2.22), the vertical wavefunction is

$$\Phi_l^{\pm}(z) = \mathbf{A}_l^{\pm} e^{\pm i\kappa(z-z_l)} \chi_l(z). \quad (2.39)$$

The vectorial character of  $\mathbf{A}_{wl}^{\pm}$  will require changes in Sec. 2.1.4. For electromagnetic radiation in nonmagnetic media, the boundary conditions at an interface with normal  $\mathbf{n}$  are [12, eq. 7.37]

$$\sum_{\pm} \bar{\epsilon} \mathbf{E}^{\pm} \mathbf{n} = \text{const}, \quad (2.40) \quad \text{{EbcE1}}$$

$$\sum_{\pm} \mathbf{E}^{\pm} \times \mathbf{n} = \text{const}, \quad (2.41) \quad \text{{EbcE2}}$$

$$\sum_{\pm} \mathbf{k}_l^{\pm} \times \mathbf{E}^{\pm} = \text{const}. \quad (2.42) \quad \text{{EbcE3}}$$

We will only consider the two polarization directions, conventionally designated as  $p$  and  $s$ , defined in Figure 2.4. As some algebra on (2.40) to (2.42) would show, these are *principal axes*, meaning that if both incoming fields  $\mathbf{E}_{l-1}^{-}$  and  $\mathbf{E}_l^{+}$  are strictly polarized in either  $p$  or  $s$  direction, then the outgoing fields  $\mathbf{E}_{l-1}^{+}$  and  $\mathbf{E}_l^{-}$  are polarized in the same direction. Conversely, if the incoming fields are mixtures of  $p$  and  $s$  polarization, then the outgoing fields will be, in general, mixed differently. Therefore if polarization factors are quantitatively important in an experiment, one should strive to accurately polarize the incident beam in  $p$  or  $s$  direction in order to avoid the extra complication of variably mixed polarizations.

Further algebra on (2.40) to (2.42) replicates the reflection law that relates  $\mathbf{k}^-$  and  $k^+$  and Snell's law (2.20). Taking these for granted, we only retain equations that are needed to determine the field amplitudes  $E^\pm$ . For  $p$  polarization they yield

$$\begin{pmatrix} k & k \\ -\kappa/k & \kappa/k \end{pmatrix} \begin{pmatrix} E^- \\ E^+ \end{pmatrix} = \text{const}, \quad (2.43) \quad \{\text{EbcE3}\}$$

and for  $s$  polarization

$$\begin{pmatrix} 1 & 1 \\ -\kappa & \kappa \end{pmatrix} \begin{pmatrix} E^- \\ E^+ \end{pmatrix} = \text{const}. \quad (2.44)$$

The latter equation can be brought into the form (2.31). In consequence,  $s$ -polarized X-rays are refracted and reflected in exactly the same ways as unpolarized neutrons.

For  $p$  polarization, ...(TODO)

## 2.2 Solution of the split boundary problem

{Ssolvsplit}

### 2.2.1 The split boundary problem

{Ssplibou}

We now consider beam propagation through the entire multilayer sample, from the semiinfinite top layer at  $l = 0$  to the semiinfinite substrate at  $l = N - 1$ , which for brevity shall be denoted by  $\nu := N - 1$ .

Let us assume that the radiation source or sink is located at  $z > 0$ . Then in the top layer,  $t_0 = 1$  is given by the incident or back-traced final plane wave. In the substrate,  $t_\nu = 0$  because there is no radiation coming from  $z \rightarrow -\infty$ . This leaves us with two unknown amplitudes, the overall coefficients of transmission  $t_\nu$  and reflection  $r_0$ . These two unknowns are connected by a system of two linear equations,

$$\begin{pmatrix} 1 \\ r_0 \end{pmatrix} = M \begin{pmatrix} t_\nu \\ 0 \end{pmatrix} \quad (2.45) \quad \{\{E1Ap\}\}$$

with the matrix product

$$M := M_1 \cdots M_\nu =: \begin{pmatrix} M_{tt} & M_{tr} \\ M_{rt} & M_{rr} \end{pmatrix}. \quad (2.46) \quad \{\{DM22\}\}$$

To apply this and all the following to the scattered beam in transmission GISAS (sink location  $z < 0$ ), we just reverse the order of layers:  $(0, \dots, \nu) \mapsto (\nu, \dots, 0)$ .

Equation (2.45) is a *split boundary problem* because the given amplitudes  $t_0 = 1$ ,  $r_\nu = 0$  appear on different sides of the equation. It can be reorganized as

$$\begin{pmatrix} t_\nu \\ r_0 \end{pmatrix} = W \begin{pmatrix} 1 \\ 0 \end{pmatrix} \quad (2.47) \quad \{\{EW1f\}\}$$

with

$$W = \mathcal{W}(M) := \begin{pmatrix} M_{tt}^{-1} & M_{tt}^{-1}M_{tr} \\ M_{rt}M_{tt}^{-1} & (M_{rr} - M_{rt}M_{tt}^{-1}M_{tr}) \end{pmatrix}. \quad (2.48) \quad \{\{EM2W\}\}$$

For later use, we note the inverse function

$$M = \mathcal{M}(W) = \begin{pmatrix} (W_{tt} - W_{tr}W_{rr}^{-1}W_{rt}) & W_{tr}W_{rr}^{-1} \\ W_{rr}^{-1}W_{rt} & W_{rr}^{-1} \end{pmatrix}. \quad (2.49) \quad \{\{EW2M\}\}$$

This formalism, originally developed for dynamic X-ray diffraction [13, 14], holds also if the matrix components are not commutative under multiplication. This will allow us later (for polarized neutrons, Chapter 4) to replace the scalar matrix components by  $2 \times 2$  matrices.

From (2.47) and (2.48), we can read off

$$t_\nu = M_{tt}^{-1} \quad \text{and} \quad r_0 = M_{rt}M_{tt}^{-1}. \quad (2.50) \quad \{\{Etfri0J\}\}$$

With this, the split boundary problem is formally solved. However, the matrix product  $M$  (2.46) is numerically unstable [14, Sects. III, IV]. Therefore, the actual computation of  $r_0$  and  $t_\nu$  is done through a recursion (Sec. 2.2.2, TODO: polarized case).

If there is one single interface ( $\nu = 1$ ), then  $M = S_1$  yields the standard Fresnel results, namely the transmitted amplitude

$$t_1 = \frac{2\kappa_0}{\kappa_0 + \kappa_1} \quad (2.51) \quad \{\{\text{EtFresnel}\}\}$$

and the reflected amplitude

$$r_0 = \frac{\kappa_0 - \kappa_1}{\kappa_0 + \kappa_1}. \quad (2.52) \quad \{\{\text{ErFresnel}\}\}$$

### 2.2.2 Recursive solution

{Srt1}

As mentioned under (2.50), the matrix product  $M$  (2.46) is numerically unstable [14, Sects. III, IV]. It is therefore preferable to solve the split boundary problem through a recursion.<sup>2</sup> Also, to compute scattering it is not sufficient to determine  $r_0$  and  $t_\nu$ ; the radiation amplitudes inside the inner layers are also needed. This is another good reason to use a recursive algorithm.

In the polarized case, we will use a recursion based on the matrix inversion (2.49) (TODO: confirm and insert link to section). In the scalar case, we use the much simpler recursion of Parratt [15]. It is based on the insight that one does not need to compute  $t_l$  and  $r_l$  separately, but only their ratio  $x_l := r_l/t_l$ . Spelling out (2.32) with  $\delta := \delta_{l-1}$  and  $s^\pm := s_l^\pm$ , we obtain

$$x_{l-1} = \frac{\delta s^- + \delta s^+ x_l}{\delta^{-1} s^+ + \delta^{-1} s^- x_l} = \delta^2 \frac{R + x_l}{1 + R x_l}. \quad (2.53) \quad \{\{\text{EParratt}\}\}$$

The second expression involves the single-interface Fresnel reflection coefficient

$$R := \frac{s^-}{s^+} = \frac{\kappa_{l-1} - \kappa_l}{\kappa_{l-1} + \kappa_l}. \quad (2.54) \quad \{\{\text{EParratt}\}\}$$

The recursion starts at the bottom with  $x_\nu = 0$ .

---

<sup>2</sup>In early versions of BornAgain, we started from the bottom with  $\tilde{t}_\nu = 1$ , and normalized the final result by division through  $\tilde{t}_0$ . For opaque samples, this algorithm fails because of arithmetic overflow. Through some versions of BornAgain, we used bisection to search for the bottom-most layer with finite transmitted intensity. Then we noted that the simple recursion can be rescued by renormalizing after each step. This turned out to be equivalent to the Parratt recursion [15].

## 2.3 Implementation

{SimplML}

Last updated to reflect the actual code in May 2023.

### 2.3.1 Call chain

All simulations are run through the virtual function `ISimulation::runComputation`.

For classes `ScatteringSimulation` and `OffspecSimulation`, most work is done in `Compute::scattered_and_reflected`,

for class `SpecularSimulation` in `Compute::reflectedIntensity`,

whereas class `DepthprobeSimulation` performs the computation directly in `runComputation`.

In function `Compute::scattered_and_reflected`,

incoming and outgoing fluxes are obtained from functions `ReSample::fluxesIn` and `fluxesOut`, and stored in instances of class `Fluxes`, which incarnates `OwnningVector<IFlux>`.

Following that, scattering is computed by functions `Compute::dwbaContribution` and `Compute::roughMultiLayerContribution`.

Specular intensity is added to the appropriate detector pixel by function `Compute::gisasSpecularContribution`.

In `DepthprobeSimulation::runComputation`, incoming fluxes are obtained from function `ReSample::fluxesIn`.

In functions `ReSample::fluxesIn` and `fluxesOut` call either `Compute::SpecularScalar::fluxes` or `Compute::SpecularMagnetic::fluxes`.

For specular simulations, function `Compute::reflectedIntensity` calls either `Compute::SpecularScalar::topLayerR` or `Compute::SpecularMagnetic::topLayerR`. These functions only return amplitudes reflected from the top of the sample, whereas the `fluxes` functions called for scattering or depthprobe simulation compute up and down travelling amplitudes for each sample layer.

Functions `fluxes` and `topLayerR` are implemented in files [ComputeFluxScalar.cpp](#) and [ComputeFluxMagnetic.cpp](#), where they share some local functions.

### 2.3.2 Scalar fluxes

The core numeric algorithm for the scalar flux computation is implemented in [ComputeFluxScalar.cpp](#). Here the code is simplified by omitting roughness and transmission geometry. The code uses class `Spinor`, which has components `u` and `v`, here representing transmitted and reflected amplitude. Interfaces are numbered as in Fig. 2.2.

```

1  std::vector<Spinor>
2  computeTR(SliceStack& slices, std::vector<cmplx>& kz)
3  {
4      // Parratt algorithm, pass 1:
5      //   compute t/t factors and r/t ratios from bottom to top.
6      size_t N = slices.size();
7      std::vector<cmplx> tfactor(N-1); // transmission damping
8      std::vector<cmplx> ratio(N);    // Parratt's x=r/t
9      ratio[N-1] = 0;
10     for (size_t i = N-1; i > 0; i--) {
11         cmplx slp = 1 + kz[i]/kz[i-1];
12         cmplx slm = 1 - kz[i]/kz[i-1];
13         cmplx delta = exp_I(kz[i-1] * slices[i-1].thicknessOr0());
14         cmplx f = delta / (slp + slm * ratio[i]);
15         tfactor[i-1] = 2 * f;
16         ratio[i-1] = delta * (slm + slp * ratio[i]) * f;
17     }
18
19     // Parrat algorithm, pass 2:
20     //   compute r and t from top to bottom.
21     std::vector<Spinor> TR(N);
22     TR[0] = Spinor(1., ratio[0]);
23     for (size_t i = 1; i < N; ++i) {
24         TR[i].u = TR[i-1].u * tfactor[i-1]; // Spinor.u is t
25         TR[i].v = ratio[i] * TR[i].u;       // Spinor.v is r
26     }
27
28     return TR;
29 }

```

{Lti}

{Lri}

There are two code blocks, each with a loop over interfaces. The first loop runs from bottom  $l = \nu$  to top  $l = 1$ . Variables `slp` and `slm` are the coefficients  $s_l^\pm$  of (2.36). Variable `delta` is  $\delta_{l-1}$  as defined in (2.29). These are used for recursively computing transmission damping factors

$$F_{l-1} := \frac{2\delta_{l-1}}{s_l^+ + s_l^- x_l} \quad (2.55)$$

and Parratt ratios (2.53)

$$x_{l-1} = \delta_{l-1} \frac{s_l^- + s_l^+ x_l}{2} F_{l-1} = \delta_{l-1}^2 \frac{s_l^- + s_l^+ x_l}{s_l^+ + s_l^- x_l}, \quad (2.56)$$

starting from the bottom value  $x_\nu = 0$ . The second loop starts from the top where  $t_0 = 1$ ,  $r_0 = 0$ . From (2.32),

$$t_{l-1} = \delta^{-1} \left( \frac{s^+}{2} t_l + \frac{s^-}{2} r_l \right) = \frac{s^+ + s^- x_l}{2\delta} t_l = F_{l-1}^{-1} t_l. \quad (2.57)$$

Bringing  $F_{l-1}$  to the other side, we obtain code line 24. By definition,  $x_l = r_l/t_l$ . Bringing  $t_l$  to the other side, we obtain code line 25.



## 3 Scattering by rough interfaces

{SRough}

The SLD decomposition (2.1) leaves some freedom how to model interface roughness. In the standard approach,  $\bar{v}(z)$  always represents the average SLD at given height  $z$ . Insofar, roughness has the same effect as an SLD gradient in a sample that is translationally invariant in the  $xy$  plane. The effect of graded SLD profiles upon reflection and transmission of a multilayer sample is discussed in Sec. 3.1.

Additionally, the horizontal inhomogeneity of a rough interface gives rise to diffuse scattering, discussed in Sec. 3.2.

By energy conservation, scattering reduces the reflected or/and transmitted intensity. How to account for these losses in the R/T computation is an open research question (TODO: link to section).

### 3.1 Propagation through graded interfaces

{Sgraded}

#### 3.1.1 Interface with tanh profile

Graded interfaces have a smooth SLD profile, i.e. the function  $\bar{v}(z)$  or  $\kappa^2(z)$  evolves continuously from one bulk value to the other. Among the SLD profiles that can be solved analytically, the tanh (Fig. 3.1a) profile is particularly important. A good summary of the solution can be found in Ch. 2.5 of Lekner [16].<sup>1</sup> Whereas Lekner only considers the electromagnetic case with a profile  $\epsilon(z)$ , we summarize the theory in terms of  $\kappa = \epsilon K^2 - k_{\parallel}^2$ .

We posit a profile

$$\kappa^2(z) = \frac{\kappa_a^2 + \kappa_b^2}{2} + \frac{\kappa_b^2 - \kappa_a^2}{2} \tanh \frac{z}{2\tau}. \quad (3.1)$$

The parameter  $\tau$  is related to the roughness length  $\sigma$  of the BornAgain API through

$$\pi\tau = \left(\frac{\pi}{2}\right)^{3/2} \sigma. \quad (3.2)$$

For reference, we note the derivative

$$\frac{d}{dz} \kappa^2(z) = \frac{\kappa_b^2 - \kappa_a^2}{4\tau} \cosh^{-2} \frac{z}{2\tau}. \quad (3.3)$$

---

<sup>1</sup>He credits Eckart (1930) and Epstein (1930) for the solution. For a short summary, see also [17, § 25, exercise 3].

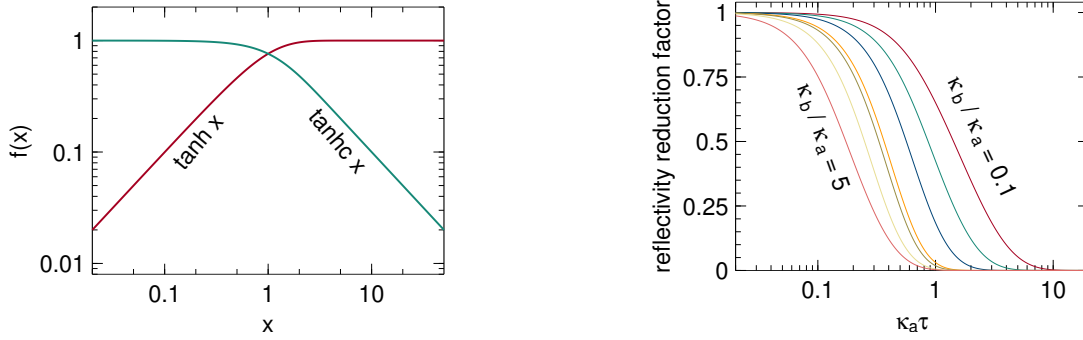


Figure 3.1: (a) Functions  $\tanh$  and  $\tanhc$ . (b) Reflectivity reduction factor, obtained by dividing (3.7) through the Fresnel reflectivity (2.51), as function of  $\kappa_a \tau$  for ratios  $\kappa_b/\kappa_a$  of 0.1, 0.2, 0.4, 0.9, 1.1, 2, and 5.

{Ftanhc}

The solution  $\Phi(z)$  involves a hypergeometric function. Here we only note the reflection coefficient [16, Eq. 2.88]

$$r_{ab} = e^{2i\varphi} \frac{\sinh \pi \tau (\kappa_a - \kappa_b)}{\sinh \pi \tau (\kappa_a + \kappa_b)}. \quad (3.4) \quad \{\text{ErTanh}\}$$

The phase  $\varphi$  is a real number as long as  $\kappa_a$  and  $\kappa_b$  are real. The transmission coefficient  $t_{ab}$  is communicated in [18]. Using various properties of the Gamma and sinh functions, one can verify flux conservation (2.37).

In the limit  $\tau \rightarrow 0$ , the phase factor  $\varphi$  in (3.4) goes to zero. For simplicity, we let  $\varphi = 0$  throughout. This approximation is equivalent to an adjustment of the interface position  $z_{ab}$  by an amount that can be expected to be small compared to the interface thickness  $\tau_{ab}$ .

To rewrite (3.4) in a form inspired by the Fresnel reflection coefficient (2.52), we use the identity

$$\frac{\sinh(x - y)}{\sinh(x + y)} = \frac{\sinh x \cosh y - \sinh y \cosh x}{\sinh x \cosh y + \sinh y \cosh x} = \frac{\tanh y - \tanh x}{\tanh y + \tanh x} \quad (3.5) \quad \{\text{ErTanh}\}$$

with  $x := \pi \tau \kappa_a$  and  $y := \pi \tau \kappa_b$ . We write  $\tanhc x := (\tanh x)/x$  (Fig. 3.1a) and define the roughness factor

$$\mathcal{R}_{ab} := \sqrt{\frac{\tanhc \pi \tau \kappa_b}{\tanhc \pi \tau \kappa_a}}. \quad (3.6) \quad \{\text{ERba}\}$$

With all this, (3.4) can be cast as

$$r_{ab} = \frac{\mathcal{R}_{ab}^{-1} \kappa_a - \mathcal{R}_{ab} \kappa_b}{\mathcal{R}_{ab}^{-1} \kappa_a + \mathcal{R}_{ab} \kappa_b}, \quad (3.7) \quad \{\text{ErTanh2}\}$$

which has the form of the Fresnel reflection coefficient (2.52), except for the factors  $\mathcal{R}_{ab}^{-1}$  and  $\mathcal{R}_{ab}$ . For  $\tau \rightarrow 0$ , these factors go to 1 so that (2.52) is fully recovered (Fig. 3.1b).

The reduced  $r_{ab}$  of (3.7) can be obtained from the basic transfer matrix equation (2.32) if the coefficients  $s^\pm$  of (2.36) are replaced by<sup>2</sup>

$$s_a^\pm = \mathcal{R}_{ab}^{-1} \pm \mathcal{R}_{ab} \kappa_b / \kappa_a. \quad (3.8) \quad \{\{\text{Es1pmTanh}\}\}$$

It is easily verified that the energy conservation (2.37) still holds.

### 3.1.2 Névot-Croce factor

The Névot-Croce factor is an exponential attenuation factor for the reflection coefficient:

$$\tilde{r}_{ab} = r_{ab} e^{-2k_a k_b \sigma_{ab}^2}, \quad (3.9) \quad \{\{\text{ErNC}\}\}$$

where  $r_{ab}$  is the Fresnel reflectivity (2.52) of a sharp interface. This form can be obtained in various ways, with more or less hand-wavy arguments or approximations. As e.g. used by Tolan it can be obtained by averaging the Parrat recursion equations over a Gaussian material profile [19], equation 2.34. The same result can also be obtained from formal perturbation theory, see e.g. [20] and references therein.

If the transmission coefficients are left unaltered, the resulting reduction in reflectivity can be interpreted as a loss into diffuse scattering channels. This interpretation is mentioned by Névot et al. [21].

More questionable is the simultaneous modification of the transmission coefficient. Currently BornAgain uses

$$\tilde{t}_{ab} = t_{ab} e^{+(k_a - k_b)^2 \sigma^2 / 2}, \quad (3.10) \quad \{\{\text{EtNC}\}\}$$

where  $t_{ab}$  is the Fresnel coefficient (2.51). This is the result obtained by Tolan [19, Eq. 2.35], and is also given by de Boer [20] as a result from formal perturbation theory in the limit of very small lateral correlation length. To obtain  $\tilde{r}_{ab}$  and  $\tilde{t}_{ab}$  from the basic transfer matrix equation (2.32), we need to replace the coefficients  $s^\pm$  of (2.36) by

$$s_l^\pm = (1 \pm \kappa_{l-1} / \kappa_l) \exp(-(\kappa_{l-1} \mp \kappa_l)^2 \sigma^2 / 2), \quad (3.11) \quad \{\{\text{Es1pmNC}\}\}$$

which is consistent with [22, Eq. 3.114].

However, the total reflected and transmitted flux  $\kappa_a |\tilde{r}_{ab}|^2 + \kappa_b |\tilde{t}_{ab}|^2$ , computed as in (2.37), is *greater* than the incoming flux  $\kappa_a$ . This takes all credibility from (3.10) and (3.11).

---

<sup>2</sup>Implemented in file [ComputeFluxScalar.cpp](#), function `transition` [30may23].

## 3.2 Scattering by a rough interface

{Sroughscatter}

Fragmentary. With contributions by Randolf Beerwerth and Walter Van Herck.<sup>3</sup>

### 3.2.1 Scattering in DWBA

{SroughDWBA}

In first-order distorted-wave Born approximation (DWBA), the scattering cross section is given by

$$\frac{d\sigma}{d\Omega} = \left| \int d^3r \Psi_i^*(\mathbf{r}) V(\mathbf{r}) \Psi_f(\mathbf{r}) \right|^2 =: |\langle \Psi_i | V | \Psi_f \rangle_{\mathbf{r}}|^2, \quad (3.12) \quad \{\text{Ecross1}\}$$

where  $V(\mathbf{r})$  is the deviation from a reference potential  $V^0(z)$  that is used to compute the distorted wave function  $\Psi$  for given incident and final far-field wave vectors  $\mathbf{k}_i, \mathbf{k}_f$ . Since the distorted waves are governed by a mean potential that only depends on  $z$ , they have the form

$$\Psi(\mathbf{r}) = e^{i\mathbf{k}_{\parallel} \mathbf{r}_{\parallel}} \Phi(z). \quad (3.13) \quad \{\text{Ecross1}\}$$

We introduce the scattering vector

$$\mathbf{q} := \mathbf{k}_f - \mathbf{k}_i \quad (3.14)$$

and the vertically integrated form factor

$$F(\mathbf{r}_{\parallel}) := \int dz \Phi_i^*(z) V(\mathbf{r}) \Phi_f(z) =: \langle \Phi_i | V | \Phi_f \rangle_z \quad (3.15) \quad \{\text{DFpa}\}$$

so that we can write (3.12) as

$$\frac{d\sigma}{d\Omega} = \int d^2r'_{\parallel} \int d^2r_{\parallel} e^{i\mathbf{q}_{\parallel}(-\mathbf{r}'_{\parallel} + \mathbf{r}_{\parallel})} F^*(\mathbf{r}'_{\parallel}) F(\mathbf{r}_{\parallel}). \quad (3.16) \quad \{\text{Ecross11}\}$$

We recast (3.16) as a Fourier transform

$$\frac{d\sigma}{d\Omega} = A \int d^2r_{\parallel} e^{i\mathbf{q}_{\parallel} \mathbf{r}_{\parallel}} G(\mathbf{r}_{\parallel}) \quad (3.17) \quad \{\text{Ecross12}\}$$

with the illuminated area  $A$  and the spatial correlation function

$$G(\mathbf{r}_{\parallel}) := A^{-1} \int d^2r'_{\parallel} F^*(\mathbf{r}'_{\parallel}) F(\mathbf{r}'_{\parallel} + \mathbf{r}_{\parallel}). \quad (3.18) \quad \{\text{DGrrpa}\}$$

---

<sup>3</sup>Ingested from ba-intern/theory on 29may23. Material was originally Roughness.tex, then ch. 4 in Stratified.tex, then again in a separate document RoughScatter.tex.

### 3.2.2 Random potential

{Srandvar}

To describe disordered interfaces, we assume that the potential depends on a random variable  $u(\mathbf{r}_{\parallel})$ :

$$V(\mathbf{r}) = V(z; u(\mathbf{r}_{\parallel})). \quad (3.19) \quad \{\text{DGrpa}\}$$

The scattering cross section (3.12) must be replaced by an average over the function  $u(\mathbf{r}_{\parallel})$ ,

$$\frac{d\sigma}{d\Omega} = \left\langle |\langle \Psi_i | V | \Psi_f \rangle_{\mathbf{r}}|^2 \right\rangle_{\{u\}}. \quad (3.20) \quad \{\{\text{Ecross2}\}\}$$

The subscripts  $\mathbf{r}$  and  $\{u\}$  could help to distinguish the quantum-mechanical and the statistical average. However, to avoid overloaded notation, we will omit them in the following. Rather, we will always use big angular brackets to mark the statistical average.

The Fourier transformed cross section can be maintained as in (3.17) provided the spatial correlation function (3.18) is redefined as

$$G(\mathbf{r}_{\parallel}) := A^{-1} \int d^2 r'_{\parallel} \left\langle F^*(u(\mathbf{r}'_{\parallel})) F(u(\mathbf{r}'_{\parallel} + \mathbf{r}_{\parallel})) \right\rangle. \quad (3.21) \quad \{\{\text{D2Grpa}\}\}$$

We now assume that the distribution of the  $u(\mathbf{r}'_{\parallel})$  and  $u(\mathbf{r}'_{\parallel} + \mathbf{r}_{\parallel})$  depends only on the distance  $\mathbf{r}_{\parallel}$ , not on the absolute location  $\mathbf{r}'_{\parallel}$ . Thereby, Equation (3.21) can be simplified as

$$G(\mathbf{r}_{\parallel}) = \left\langle F^*(u(0)) F(u(\mathbf{r}_{\parallel})) \right\rangle. \quad (3.22) \quad \{\{\text{D2Grpa2}\}\}$$

The average involves a two-point correlation function  $P_2(u, v; \mathbf{r}_{\parallel})$ :

$$G(\mathbf{r}_{\parallel}) = \int du \int dv P_2(u, v; \mathbf{r}_{\parallel}) F^*(u) F(v). \quad (3.23) \quad \{\text{D2Grpa2}\}$$

We anticipate that the limiting behavior of  $P_2$  is governed by the one-point distribution function  $P_1$ ,

$$P_2(u, v; \mathbf{r}_{\parallel}) \rightarrow \begin{cases} P_1(u) \delta(u - v) & \text{for } \mathbf{r}_{\parallel} \rightarrow 0, \\ P_1(u) P_1(v) & \text{for } \mathbf{r}_{\parallel} \rightarrow \infty. \end{cases} \quad (3.24)$$

### 3.2.3 Covariance ex machina

{Scov}

In the pioneering paper by Sinha et al. [23] and in much of the subsequent literature [24], the scattering cross section is defined differently from Equation (3.20), namely as the covariance

$$\left. \frac{d\sigma}{d\Omega} \right|_{\text{cov}} := \text{Cov}_{\{u\}} \left( \langle \Psi_i | V | \Psi_f \rangle^*, \langle \Psi_i | V | \Psi_f \rangle \right) \equiv \left\langle |\langle \Psi_i | V | \Psi_f \rangle|^2 \right\rangle - \left| \left\langle \langle \Psi_i | V | \Psi_f \rangle \right\rangle \right|^2. \quad (3.25) \quad \{\{\text{DcrossCov}\}\}$$

To compensate for the negative extra term, there must be another cross section

$$\left. \frac{d\sigma}{d\Omega} \right|_{\text{T/R}} := \left| \left\langle \langle \Psi_i | V | \Psi_f \rangle \right\rangle \right|^2 \quad (3.26) \quad \{\{\text{DcrossRT}\}\}$$

$$= A \int d^2 r_{\parallel} e^{i\mathbf{q}_{\parallel} \mathbf{r}_{\parallel}} \left\langle F(0) \right\rangle^* \left\langle F(\mathbf{r}_{\parallel}) \right\rangle. \quad (3.27) \quad \{\text{DcrossRT}\}$$

The one-point averages are governed by the distribution function  $P_1(u)$  that does not depend on horizontal location. Hence

$$\left. \frac{d\sigma}{d\Omega} \right|_{\text{T/R}} = A \int d^2 r_{\parallel} e^{i\mathbf{q}_{\parallel} \mathbf{r}_{\parallel}} \left| \left\langle F \right\rangle \right|^2 \quad (3.28) \quad \{\{\text{EcrossRT2}\}\}$$

$$= A(2\pi)^2 \delta(\mathbf{q}_{\parallel}) \left| \left\langle F \right\rangle \right|^2. \quad (3.29) \quad \{\text{EcrossRT2}\}$$

This cross section is only nonzero if  $\mathbf{q}_{\parallel} = 0$ . Elastic scattering must fulfill  $k_f = k_i$ . Together, these conditions imply  $k_{iz} = \pm k_{fz}$ , which is only satisfied by the direct (transmitted) and by the specular (reflected) beam. For this reason, the cross section (3.26) has been labelled “R/T”.

In the present context, we are only interested in scattering out of the transmitted or reflected beam. Therefore we can ignore the R/T cross section (3.26), and substitute the covariance (3.25) for the original cross section (3.12). We will see that this simplifies computations. So we replace (3.17) by

$$\left. \frac{d\sigma}{d\Omega} \right|_{\text{T/R}} = A \int d^2 r_{\parallel} e^{i\mathbf{q}_{\parallel} \mathbf{r}_{\parallel}} \Delta G(\mathbf{r}_{\parallel}) \quad (3.30) \quad \{\{\text{EcrossDG}\}\}$$

with the modified correlation function (3.22)

$$\Delta G(\mathbf{r}_{\parallel}) := \text{Cov}\left(F^*(u(0)), F(u(\mathbf{r}_{\parallel}))\right) \quad (3.31) \quad \{\{\text{DDGrpa}\}\}$$

$$= \int du \int dv \Delta P_2(u, v; \mathbf{r}_{\parallel}) F^*(u) F(v). \quad (3.32) \quad \{\text{DDGrpa}\}$$

The integral involves the distribution function

$$\Delta P_2(u, v) := P_2(u, v) - P_1(u)P_1(v). \quad (3.33) \quad \{\{\text{DDP2}\}\}$$

### 3.2.4 Sharp, rough interface

\{\{\text{Sinterface}\}\}

We consider a sharp transition between two different materials that takes place at a rough interface located at height  $z = u(\mathbf{r}_{\parallel})$ . The scattering potential is the difference

$$V(\mathbf{r}) = V_u(z; u(\mathbf{r}_{\parallel})) - V^0(z) \quad (3.34) \quad \{\{\text{EVasdiff}\}\}$$

between the actual potential for a given interface profile  $u$

$$V_u(z; u) := \frac{V_a + V_b}{2} + \frac{V_a - V_b}{2} \text{sgn}(z - u) \quad (3.35) \quad \{\text{EVasdiff}\}$$

and the reference potential

$$V^0(z) := \frac{V_a + V_b}{2} + \frac{V_a - V_b}{2} s_0(z) \quad (3.36)$$

that has been used to compute the vertical wave functions  $\Phi_i, \Phi_f$ , and therefore does not contribute to scattering. The constants  $V_a, V_b$  are the values of  $V^0$  in the bulk *above* and *below* the interface, denoted by layer indices a and b. The profile function  $s_0(z)$  has the limits  $s_0(\pm\infty) = \pm 1$ . We rewrite (3.34) as

$$V(\mathbf{r}) = (V_b - V_a) \mathcal{V}(z; u(\mathbf{r}_{\parallel})) \quad (3.37)$$

with the dimensionless difference potential

$$\mathcal{V}(z, u) := \frac{1}{2} [\text{sgn}(z - u) - s_0(z)]. \quad (3.38) \quad \{\text{DVddp}\}$$

To get rid of a constant prefactor, we rewrite the correlation function (3.31) as

$$\Delta G(\mathbf{r}_{\parallel}) = |V_b - V_a|^2 \Delta g(\mathbf{r}_{\parallel}) \quad (3.39) \quad \{\text{E31Grpa}\}$$

with the reduced correlation function

$$\Delta g(\mathbf{r}_{\parallel}) := \text{Cov}\left(f^*(u(0)), f(u(\mathbf{r}_{\parallel}))\right) = \int du \int dv \Delta P_2(u, v; \mathbf{r}_{\parallel}) f^*(u) f(v) \quad (3.40) \quad \{\text{DDgrpa}\}$$

and the reduced vertical form factor

$$f(u) := \int dz \Phi_i^*(z) \mathcal{V}(z; u) \Phi_f(z). \quad (3.41) \quad \{\text{Dfpa}\}$$

### 3.2.5 Stepwise reference potential

To facilitate computations, we approximate the smooth function  $s_0(z)$  by a step function that takes  $J$  different values  $s_j$ , with layer index  $j$  running from  $b = 1$  to  $a = J$ . We decompose the vertical wave function  $\Phi_d$  (with  $d = i, f$ ) as

$\{\text{Sstepwise}\}$

$$\Phi_d(z) = \sum_{j=1}^J [z \in \mathcal{L}_j] \Phi_{dj}(z), \quad (3.42) \quad \{\text{Dfpa}\}$$

where  $\mathcal{L}_j$  denotes the  $z$  interval occupied by layer  $j$ . Within one layer, the vertical wave function consists of two exponentials with constant coefficients,

$$\Phi_{dj}(z) = t_{dj} e^{-i\kappa_{dj} z} + r_{dj} e^{i\kappa_{dj} z}. \quad (3.43) \quad \{\text{2EPhijz}\}$$

To prepare for summation over downward and upward travelling waves, we rewrite (3.43) as

$$\Phi_{dj}(z) = \sum_{\alpha=-1, +1} c_{dj\alpha} e^{i\kappa_{dj\alpha} z} \quad (3.44) \quad \{\text{EPhidj}\}$$

with  $c_{dj-} := t_{dj}$ ,  $c_{dj+} := r_{dj}$ , and  $\kappa_{j\pm} := \pm\kappa_j$ . With the further definitions

$$q_{j\alpha\beta} := \kappa_{fj\alpha} - \kappa_{ij\beta}, \quad (3.45)$$

$$B_{j\alpha\beta} := c_{ij\alpha}^* c_{fj\beta}, \quad (3.46)$$

the wave function product in (3.41) becomes

$$\Phi_i^*(z)\Phi_f(z) = \sum_j [z \in \mathcal{L}_j] \sum_{\alpha}^{-,+} \sum_{\beta}^{-,+} B_{j\alpha\beta} e^{iq_{j\alpha\beta}z}. \quad (3.47)$$

Diffuse scattering is governed by the dimensionless difference potential (3.38), which can be written

$$\mathcal{V}(z, u) := \frac{1}{2} [\text{sgn}(z - u) - s_{j(z)}] \quad (3.48) \quad \{\text{EVddpstep}\}$$

with a function  $j(z)$  that yields the layer index for a given vertical coordinate  $z$ .

### 3.2.6 One-step reference potential

\{\text{Sonestep}\}

We now choose a reference potential that has a single step at  $z = 0$ . In this case, the profile function is just  $s_0(z) = \text{sgn}(z)$ . The dimensionless difference potential (3.38) and (3.48) can be further simplified to take the form

$$\mathcal{V}(z; u) = [0 < z < u] - [u < z < 0], \quad (3.49) \quad \{\text{EVddpstep}\}$$

with the Iverson-Knuth indicator bracket defined by  $[\text{false}] = 0$  and  $[\text{true}] = 1$ . After some rearrangement we find

$$f(u) = \sum_j^{\text{b,a}} [u \in \mathcal{L}_j] \sum_{\alpha}^{-,+} \sum_{\beta}^{-,+} B_{j\alpha\beta} \int_0^u dz e^{iq_{j\alpha\beta}z}. \quad (3.50) \quad \{\text{Efujab}\}$$

From here on, it is convenient to work with a bundled index  $\mu \equiv (\alpha, \beta)$  that runs from 0 to 3 and stands for the four possible combinations of  $\pm\pm$ . With the further abbreviation

$$A_{j\mu} := B_{j\mu}/q_{j\mu}, \quad (3.51) \quad \{\text{DA}\}$$

the result of carrying out the integral in (3.50) can be written as

$$f(u) = \sum_j^{\text{b,a}} [u \in \mathcal{L}_j] \sum_{\mu}^{\pm\pm} \frac{A_{j\mu}}{i} (e^{iq_{j\mu}u} - 1). \quad (3.52) \quad \{\text{DA}\}$$

The reduced correlation function (3.40) is just the covariance of  $f^*(u(0))$  and  $f(u(\mathbf{r}_{\parallel}))$ . Only terms that involve both  $u(0)$  and  $u(\mathbf{r}_{\parallel})$  contribute. This leaves us with

$$\Delta g(\mathbf{r}_{\parallel}) = \sum_j^{\text{b,a}} \sum_k^{\text{b,a}} \sum_{\mu}^{\pm\pm} \sum_{\nu}^{\pm\pm} A_{j\mu}^* A_{k\nu} D_{j\mu, k\nu}(\mathbf{r}_{\parallel}) \quad (3.53) \quad \{\text{EDgrpa1}\}$$



with

$$D_{j\mu,k\nu}(\mathbf{r}_{\parallel}) := \int_{\mathcal{L}_j} du \int_{\mathcal{L}_k} dv \Delta P_2(u, v; \mathbf{r}_{\parallel}) e^{-iq_{j\mu}u + iq_{k\nu}v}. \quad (3.54) \quad \{\text{DD4}\}$$

If the vertical scattering wavenumbers  $q$  are real, then  $D_{j\mu,k\nu}^* = D_{k\nu,j\mu}$ . This allow us to compute (3.53) as

$$\Delta g(\mathbf{r}_{\parallel}) = \sum_{j\mu} |A_{j\mu}|^2 D_{j\mu,j\mu}(\mathbf{r}_{\parallel}) + \sum_{j\mu < k\nu} 2\text{Re } A_{j\mu}^* A_{k\nu} D_{j\mu,k\nu}(\mathbf{r}_{\parallel}). \quad (3.55) \quad \{\text{EDgrpa1c}\}$$

The operator  $<$  under the second sum refers to some lexical ordering of the indices that is used to preclude double counts.

### 3.2.7 Gaussian roughness

\{\text{SGauss}\}

From this point on, we assume a specific distribution function  $P_2$ , namely a bivariate normal distribution [25]. For brevity, we shall use the standard normal distribution

$$N_1(X) := \frac{1}{\sqrt{2\pi}} \exp\left(-\frac{X^2}{2}\right), \quad (3.56) \quad \{\text{EDgrpa1c}\}$$

and the standard bivariate normal distribution [25]

$$N_2(X, Y; \rho) := \frac{1}{2\pi\sqrt{1-\rho^2}} \exp\left[-\frac{X^2 + Y^2 - 2\rho XY}{2(1-\rho^2)}\right] \quad (3.57) \quad \{\text{DN2}\}$$

$$= N_1\left(\frac{Y+X}{\sqrt{2(1+\rho)}}\right) N_1\left(\frac{Y-X}{\sqrt{2(1-\rho)}}\right) \quad (3.58) \quad \{\text{EN2fac}\}$$

with  $\rho < 1$ . For  $\rho \rightarrow 1$ , one can see from (3.58) that  $N_2(X, Y)$  goes to  $N_1(X)\delta(X-Y)$ . We now choose

$$P_1(u) := N_1\left(\frac{u}{\sigma}\right) \quad (3.59) \quad \{\text{EN2fac}\}$$

and

$$P_2(u, v; \mathbf{r}_{\parallel}) := N_2\left(\frac{u}{\sigma}, \frac{v}{\sigma}; \rho(\mathbf{r}_{\parallel})\right). \quad (3.60)$$

The standard deviation  $\sigma$  characterizes the vertical extent of interface fluctuations. It is undifficult to verify that

$$\int dv P_2(u, v; \mathbf{r}_{\parallel}) = P_1(u) \quad (3.61)$$

for whatever  $\rho(\mathbf{r}_{\parallel})$ . Physics dictates that  $0 \leq \rho(\mathbf{r}_{\parallel}) < 1$  for  $\mathbf{r}_{\parallel} \neq 0$ , and  $\rho(0) = 1$ . A specific horizontal correlation function  $\rho(\mathbf{r}_{\parallel})$  will be chosen later.

The covariance distribution function (3.33) is given by

$$\Delta P_2(u, v; \mathbf{r}_{\parallel}) = \Delta N_2\left(\frac{u}{\sigma}, \frac{v}{\sigma}; \rho(\mathbf{r}_{\parallel})\right) \quad (3.62) \quad \{\text{EDP2}\}$$

with

$$\Delta N_2(X, Y; \rho) := N_2(X, Y; \rho) - N_1(X)N_1(Y) \quad (3.63)$$

$$\begin{aligned} &= N_1 \left( \frac{Y+X}{\sqrt{2(1+\rho)}} \right) N_1 \left( \frac{Y-X}{\sqrt{2(1-\rho)}} \right) \\ &\quad - N_1 \left( \frac{Y+X}{\sqrt{2}} \right) N_1 \left( \frac{Y-X}{\sqrt{2}} \right), \end{aligned} \quad (3.64) \quad \{\text{EDN2fac}\}$$

which has the small  $\rho$  expansion

$$\Delta N_2(X, Y; \rho) = N_1(X)N_1(Y) [\rho XY + \mathcal{O}(\rho^2)]. \quad (3.65) \quad \{\text{EDN2lin}\}$$

### 3.2.8 Analytic plane waves approximation

`\{\text{SSinhaApprox}\}`

The evaluation of the correlation function (3.53) can be simplified decisively if the wave functions  $\Phi_d$  ( $d = \text{i, f}$ ) in the vertical form factor (3.15) are approximated by two exponential functions with constant amplitudes. This amounts to omitting the  $j$  dependences in (3.44). In the literature, it is typically achieved by analytic continuation of the wavefunction of the upper layer,  $\Phi_{da}$ , into the lower layer b, or vice versa. According to Pynn [26, p. 605], this approximation is implicit in the reflectivity theory of Névot and Croce [27]. Sinha et al. [23, following Eq. 4.37] introduced for the DWBA computation of diffuse scattering. Holý et al. [24] suggest to compute the scattering intensity twice, with  $\Phi_{da}$  approximated by  $\Phi_{db}$ , and vice versa. The approximation is valid if the two results agree within requested precision.

Under this assumption we can omit the layer index from  $B, q, A$ . The sums over  $j, k$  in (3.53) become trivial, the integrals over  $u, v$  are no longer restricted to layers, and the problem reduces to

$$\Delta g(\mathbf{r}_{\parallel}) = \sum_{\mu}^{\pm\pm} \sum_{\nu}^{\pm\pm} A_{\mu}^* A_{\nu} \int du \int dv \Delta P_2(u, v; \mathbf{r}_{\parallel}) e^{-iq_{\mu}u + iq_{\nu}v}. \quad (3.66) \quad \{\text{EDgrpaS1}\}$$

With (3.62) and (3.64), the solution is straightforward [23, Eq. 4.42]:

$$\Delta g(\mathbf{r}_{\parallel}) = \sum_{\mu}^{\pm\pm} \sum_{\nu}^{\pm\pm} A_{\mu}^* A_{\nu} \left[ e^{\sigma^2 q_{\mu} q_{\nu} \rho(\mathbf{r}_{\parallel})} - 1 \right] e^{-\sigma^2 (q_{\mu}^2 + q_{\nu}^2)/2}. \quad (3.67) \quad \{\text{EDgrpaS2}\}$$

For small  $\rho$ , the difference in the bracket can be linearized in  $\rho$ . Recalling that  $A = B/q$  (3.51), we obtain [23, Eq. 4.43]

$$\Delta g(\mathbf{r}_{\parallel}) \doteq \rho(\mathbf{r}_{\parallel}) \sigma^2 \sum_{\mu}^{\pm\pm} \sum_{\nu}^{\pm\pm} B_{\mu}^* B_{\nu} e^{-\sigma^2 (q_{\mu}^2 + q_{\nu}^2)/2}. \quad (3.68) \quad \{\text{EDgrpalin}\}$$

### 3.2.9 Refracted waves, linearized correlation

We now reconsider the problem of computing the correlation function (3.53) based on wave functions that account for refraction and reflection by the mean interface, and therefore are plane waves only within one layer. In other words, we proceed without Sinha's approximation of Section 3.2.8.

Instead, to make the problem computationally accessible, we use (3.65) to linearize in  $\rho$  from the onset. So approximate (3.54) as

$$D_{j\mu,k\nu}(\mathbf{r}_{\parallel}) \doteq \rho(\mathbf{r}_{\parallel}) \sigma^2 E_j^*(q_{j\mu}) E_k(q_{k\nu}) \quad (3.69) \quad \{\text{EDgrpa2}\}$$

with the shorthand

$$E_j(q) := \int_{\mathcal{L}_j} d\frac{u}{\sigma} N_1\left(\frac{u}{\sigma}\right) \frac{u}{\sigma} e^{iqu}. \quad (3.70) \quad \{\text{EDgrpa2}\}$$

Recall that  $j$  and  $k$  take the values b, a. The layers cover the semiinfinite intervals  $\mathcal{L}_b = (-\infty, 0)$  and  $\mathcal{L}_a = (0, \infty)$ , hence

$$E_a(q) = \int_0^\infty dU N_1(U) U e^{iq\sigma U}, \quad E_b(q) = -E_a(-q). \quad (3.71)$$

Use partial integration to obtain

$$E_a(q) = \frac{1}{\sqrt{2\pi}} + \frac{iq\sigma}{2} \operatorname{erfcx}\left(\frac{-iq\sigma}{\sqrt{2}}\right), \quad (3.72)$$

$$E_b(q) = -\frac{1}{\sqrt{2\pi}} + \frac{iq\sigma}{2} \operatorname{erfcx}\left(\frac{iq\sigma}{\sqrt{2}}\right) \quad (3.73)$$

with the compensated complementary error function (function  $w(iz)$  of Abramowitz and Stegun [28, 7.1.3])

$$\operatorname{erfcx}(z) := e^{z^2} \operatorname{erfc}(z). \quad (3.74)$$

If we make the additional assumption that  $B, q, A$  are layer independent, as in Sinha's plane-waves approximation, then it is straightforward to recover the linearized result (3.68) from the previous section.

### 3.2.10 Horizontal correlations

*This is a verbatim copy of Sect. 5.6 from our reference paper [1], except for notes in boldface or italics.*

The reduction of reflected and transmitted intensity is described by the Névot-Croce factor [27]. IsGISAXS supports this loss factor, but not the diffuse scattering.

In BornAgain, diffuse scattering and beam attenuation are computed consistently. **[Not yet! This needs urgently to be implemented.]** The roughness model is taken from Ref. [29]. The height  $h$  is assumed to be a Gaussian random variable. The correlation function at in-plane distance  $R$  is (I:21)

$$C(R) := \langle h(0)h(R) \rangle = \sigma^2 e^{-(R/\xi)^{2H}}. \quad (3.75)$$

*This model has been introduced into the field of X-ray reflectivity by Sinha et al [23]. Compare their Eqns. 2.9 and 2.23.*

The user needs to specify the amplitude  $\sigma$ , the correlation length  $\xi$ , and the Hurst parameter  $H$ . The latter is restricted to  $0 < H \leq 1$ . According to Ref. [29], it defines the fractal box dimension  $D = 3 - H$  of the interface: The smaller  $H$ , the more jagged the interface (see Fig. I:7). *Again, the better reference is [23], and work cited therein.*

If there are two or more interfaces, then their height profiles may be correlated. Following again Ref. [29], this is specified through a vertical cross correlation length  $\xi_{\perp}$  that governs the correlations between two interfaces  $j$  and  $k$ , (I:22)

$$\langle h_j(0)h_k(R) \rangle = \frac{1}{2} \left[ \frac{\sigma_k}{\sigma_j} C_j(R) + \frac{\sigma_j}{\sigma_k} C_k(R) \right] e^{-|z_j - z_k|/\xi_{\perp}}. \quad (3.76)$$

### 3.3 Literature review: reflectivity and scattering from rough surfaces

Scattering from a rough surface has been studied first at a macroscopic level, for sound and radar waves (see books in TUM OPAC; see references in [30]). For light scattering literature, see Refs. 1–26 in [31].

**Steyerl 1972 [30]:** First detailed discussion of neutron reflection from rough surfaces. Main application interest is total reflection in neutron guides. Unperturbed potential is step function. Wave equation in integral form; Green's functions, ascribed to saddle point method, appear in Eqns. 15,16 without derivation; explicit expressions for all four cases  $z, z' \leq 0$  are given with some more computational details in [32, Eqn. 29]. Compact and credible expressions for upward and downward scattering in Eqns. 20,21. Result for reflected and transmitted intensity thoroughly analysed and criticised by Pynn [26]: neglect of phase factor makes approximation irrelevant for reflectometry.

**Nénot & Croce 1980 [27]:** Experimental X-ray study. Highly cited. Attenuation of the reflected beam described by the *Nénot-Croce factor* [Eqn. 3]. Theoretical section is hard to read; starts from previous results of Croce et al; claims to be self-consistent (auto-cohérente, p. 764). The key results of this work are rederived in much shorter, clearer, and more standard ways by Pynn [26] who also explicates which approximations were made.

**Beckmann and Spizzichino 1987 [33]:** Book about radar reflections; almost entirely concerned with wavelengths shorter than local radius of curvature, irrelevant for reflectometry [26].

**Sinha et al 1988 [23]:** Top-cited paper. Sects. II and III are in Born Approximation, with application e. g. to powders. Application to liquid interface. They consider only single interfaces. Grazing incidence and DWBA come in Sect. IV. For  $q_z \geq q_c$ , a small- $q$  expansion reproduces the Nénot-Croce factor. For  $q_z < q_c$ , on the other hand,  $|R| < 1$  is not found: 1st-order DWBA violates the optical theorem; the 2nd order would be needed, but is not worked out. Pynn [26, Eqn. 10] criticizes the forward scattering term [23, Eqn. 4.12], which involves the wrong incoming eigenfunction (for the plane instead of the rough surface).

**Pynn 1992 [26]:** A critical review of previous work, especially Steyerl [30], Nénot & Croce [27], and Sinha et al [23]. Nénot & Croce got the reflectivity essentially right, except for reflection coefficients smaller than  $10^{-5}$  [p. 605]. Also discusses correlated interfaces.

**Holý & al 1993 [24]:** Concerned with multilayer reflectivity and diffuse scattering. Very readable summary and extension of Sinha theory. They write the perturbation Hamiltonian of a multilayer system as a sum of single-layer contributions. This splits up into a sum of four terms, similar to the expression Walter uses. They have only four terms as they assume that the fields are identical directly below and above the interface. Walter drops this condition and hence gets twice the terms with different averaging below and above the interface. As a consequence of writing the Hamiltonian as a sum of single interface contributions, diffuse scattering leads to a double sum with the covariances appearing. Here correlation models come in. They

introduce two of them: one without and the second with vertical correlation.

Summarized and extended to periodic multilayers by Holý & Baumbach [34]. Holý & al also contributed to the book [35]; in particular, chapter 11 could be interesting.

**de Boer 1994 [36]:** Purely theoretical description of specular reflectivity on single rough interfaces. Second order DWBA calculations of the reflection and transmission coefficients in the  $T$ -matrix formalism. The resulting expressions include the lateral correlation and are shown to have the Névot-Croce factor as a limiting value for small correlation length (i.e. negligible diffuse scattering). For large correlation length, the Debye-Waller like factor is recovered, while for intermediate correlation length an interpolation factor needs to be evaluated. This factor includes a two-dimensional surface integral. For a suitably chosen correlation function, it can be reduced to a one-dimensional integral which facilitates numeric evaluation.

**de Boer & Leenaers 1996 [20]:** Survey article that briefly summarizes results from several other articles. Explains under which limiting conditions results are applicable. Gives formulae of the Fresnel coefficients for both reflection and transmission on a single interface. Névot-Croce recovered as limit of small correlation lengths, can also serve for multilayer calculations. This limit corresponds to weak scattering and can be compared to graded interfaces, i.e. the numerical approximation via Slicing that completely neglects diffuse scattering. Mentions DWBA leading to intensities greater than unity below the critical angle, introduce Rayleigh method to circumvent this. This leads to another expression for the Fresnel coefficients for large correlation lengths, that can also be applied to multilayers.

Introduce an expression for the Fresnel coefficients for intermediate correlation lengths, that relates to the lateral correlation function. Only approximately applicable to multilayers, give reference to other 1996 paper [37].

Suggest interpolation approach to treat the fields in the vicinity of an interface.

Suggest also other starting points for the perturbative approach, namely to use already corrected Fresnel coefficients or graded interfaces. Here, they specifically mention the tanh profile as implemented in BornAgain.

Other potentially interesting papers from the same author: [38] [36]

The lateral correlation function implemented in BornAgain is taken from the paper [39].

**de Boer 1996 [37]:** Deals with multilayers and considers the effects of roughness in both specular reflectivity and diffuse scattering. Employs the  $T$ -matrix formalism to compute corrections in the DWBA up to second order, rather hard to understand and result not easily usable (for me, rb). Uses flat interfaces as the starting point for perturbation theory in Section II and graded interfaces in Section III. The latter is rather vague and hard to grasp. Results are presented, dominantly for x-ray fluorescence.

Concludes that as a starting point for the DWBA graded interfaces should be used, if both the reflectivity as well as the roughness are reasonably large. Suggests an interpolation method for the fields as a starting point for the DWBA, as the field obtained from Névot-Croce factors are wrong in the vicinity of interfaces.

Claims that the second-order term for diffuse scattering is generally negligible, except when the reflectivity is large as well as for large lateral correlation length and roughness. For specular reflection, mentions the first and second order contribution to

be of the same order in the roughness and is hence only negligible for small roughnesses. However, stresses that the DWBA is only valid for small roughness values or far above the critical wave vector. Their way of extrapolating [36] the results is only valid for single interfaces or very large perpendicular correlation.

Also mentions that he is not aware of any samples, where the second order contribution has to be considered and that the theory is completely untested.

**Caticha 1995 [40]:** Studies graded interface with roughness.

**Rauscher et al 1995 [41]:** Combine the roughness theory of Sinha et al [23] with bulk density fluctuations for different geometries, thereby specializing the generic formalism of Dietrich and Haase [42].

**Ogura & Takahashi 1996 [43]:** Scattering and reflection from a random surface in the language of mathematical physics, using Itô stochastic functionals. The surface has 100% reflectance (Eqns. 3.9–10), so they miss the most difficult aspects of the problem. Possibly a starting base for collaboration with mathematical physicists; otherwise without practical value for us.

**Toperverg et al 2000 [44]:** A short note on the *optical theorem* that ensures energy conservation under reflection, transmission and scattering. The only cited literature is Sinha et al 1988 [23] and de Boer 1994–96 [36, 39, 37]. For second-order DWBA they refer to a preprint by Toperverg et al 1997 (request pending). This paper drew our attention to the optical theorem, but is most probably made obsolete by other publications that work out more details.

**Fuji 2010: [45]:** Seems to be the initial claim, that the Parrat formalism as it is currently used with roughness included in the Fresnel coefficients assumes flux conservation and hence cannot account for losses due to roughness. Detailed derivation of a modified Parrat formula that contains both Fresnel  $r$  and  $t$  coefficients. Gives examples where unphysically deep fringes are removed by their new formula. The same example does indeed seem to show weird behavior that depending on the amount of roughness deep minima change their position.

**Fuji 2013: [46]:** They derive (short) a different version of the the Parrat recursion which does not imply conservation of flux. The claim is that this reduces deep unphysical minima in Kissieg fringes when roughness is added.

**Fujii 2014: [47]:** Presents a modified version of the Parrat formula, that explicitly depends on the Fresnel *transmission* coefficients. If conservation of the flux is imposed, his formula reduces to the well-known Parrat formula, where only the Fresnel *reflection* coefficient is present. More mathematical derivation of the approach is presented in [46]. Numerical results are presented for an example, where the author shows that the usual formula yields very good results for roughness parameters that do not agree with independent experimental results (TEM). His modified formula yields good agreement with the independently verified roughness parameters. The applied transmission coefficients are given without much explanation, but the given expression kind of resembles the expressions given by Tolan [19] for the large correlation length limit.

**Fujii 2015: [48]:** Computes effective roughness factors, where the lateral correlation is considered. Obtains an expression that again resembles equations (2.40) and (2.41) in the book by Tolan[19], however, with an effective roughness. Claims good

agreement with AFM measurements.

**Chukhovskii 2011 & 2012 [49, 50]:** Claims that DWBA is inapplicable for large roughness rms  $\sigma$ . As an alternative, develops *self-consistent wave approximation* (SCWA). Starting from a Green function [49, Eqn. 4], the derivation of the scattering cross section [49, Eqn. 20] and of the reflected intensity [49, Eqn. 19] looks relatively straightforward. Subsequent averages of random functions for the standard Gaussian surface model, however, lead to very long expressions [49, Eqns. 22,23]. The optical theorem is only satisfied in the limit of large surface correlation lengths ( $k\xi\vartheta^2 \gg 1$ ) [50].

TODO <https://doi.org/10.1107/S2053273315016666> (2015)

TODO <https://www.nature.com/articles/s41598-020-68326-2> (2020)

**Chukhovskii & Roshchin 2015 [51]:** Yet another alternative to DWBA: expansion in q-eigenfunctions of the plane-surface problem.

**Maruyama, Yamazaki & Soyama 2018 [52]:** Conference proceeding, where the authors present actual computational results applying the theory from de Boer [36, 37], i.e. DWBA in second order to the specular reflectivity of multilayers. Comparison to the Névot-Croce factor, as well as contributions of the first and second order perturbation contribution. Their chosen example is very close to the Ti-Ni multilayer sample that was often considered by BA team members so far and could serve as an interesting test case for testing and comparing numerical results.

**Hafner 2019 [53]:** Contains simulations and experimental data of off-specular simulations where the contributions from specular reflection and scattering are put on a common scale. Cross sections are incoherently added, with geometric corrections arising from detector resolution and spread in angles/wavelengths. Mentions approximation valid for small scattered intensities. Summarizes statistical treatment of rough interfaces, similar correlation approach as in BornAgain.



## 4 Polarized wave propagation and scattering

{SPol}

In this chapter, we generalize our treatment of wave propagation and grazing-incidence small-angle scattering to polarized neutrons. We therefore need to study spinor wave equations, in contrast to the scalar theory of the previous chapters.

### 4.1 Polarized neutrons in 2+1 dimensions

{Snpol0}

#### 4.1.1 Schrödinger equation for neutron spinors

{SnSpinor}

In presence of a magnetic field, the propagation of free neutrons becomes spin dependent. Therefore the scalar wavefunction of Sec. 1.1.1 must be replaced by spinor  $\Psi$ . The Zeeman energy is given by the operator  $-\gamma_n \mu_{\text{nucl}} \mathbf{B} \hat{\boldsymbol{\sigma}}$  with the neutron gyromagnetic factor  $\gamma_n \simeq -1.91$ , the nuclear magneton  $\mu_{\text{nucl}}$ , the magnetic induction  $\mathbf{B}$  and the Pauli vector  $\hat{\boldsymbol{\sigma}}$ , composed of the three Pauli matrices. With the unsigned magnetic moment of the neutron,  $\mu_n := |\gamma_n \mu_{\text{nucl}}|$ , the Schrödinger equation (1.1) becomes

$$\left\{ -\frac{\hbar^2}{2m} \nabla^2 + V(\mathbf{r}) + \mu_n \mathbf{B}(\mathbf{r}) \hat{\boldsymbol{\sigma}} - \hbar\omega \right\} \Psi(\mathbf{r}) = 0. \quad (4.1) \quad \{\text{EHSchrodi}\}$$

According to Ref. [54], the magnetic field is usually applied parallel to the sample surface, but we do not rely on this.

We abbreviate the nuclear and the magnetic scattering-length density as

$$\rho^{\text{N}}(\mathbf{r}) := v_{\text{nucl}}(\mathbf{r}) \quad \text{and} \quad \rho^{\text{M}}(\mathbf{r}) := \frac{m\mu_n}{2\pi\hbar^2} B(\mathbf{r}), \quad (4.2) \quad \{\text{EHSchrodi}\}$$

and we write  $\check{\mathbf{B}}$  for the unit vector in direction of the magnetic field  $\mathbf{B}$ . So the total reduced potential is given by the operator

$$\hat{v}(\mathbf{r}) := \rho^{\text{N}}(\mathbf{r}) + \rho^{\text{M}}(\mathbf{r}) \check{\mathbf{B}}(\mathbf{r}) \hat{\boldsymbol{\sigma}}, \quad (4.3)$$

and we can rewrite the Schrödinger equation in analogy to (4.4) as

$$\{\nabla^2 + K^2 - 4\pi\hat{v}(\mathbf{r})\} \Psi(\mathbf{r}) = 0. \quad (4.4) \quad \{\text{ESchrodi2}\}$$

### 4.1.2 Propagation in a multilayer

{Smulayer2}

In the decomposition (2.1), both terms may become operators acting in spin space,

$$\hat{v}(\mathbf{r}) =: \hat{v}(z) + \delta\hat{v}(\mathbf{r}). \quad (4.5) \quad \{\{\text{Edecompose\_z2}\}\}$$

The unperturbed distorted wave has the form

$$\Phi(\mathbf{r}) = e^{i\mathbf{k}_{\parallel}\mathbf{r}_{\parallel}} \Phi(z). \quad (4.6) \quad \{\{\text{Edecompose\_z2}\}\}$$

The horizontal wave vector  $\mathbf{k}_{\parallel}$  is constant across layers. This motivates us to introduce the vertical vacuum wavenumber  $\kappa_0 := \sqrt{K^2 - k_{\parallel}^2}$ . The vertical spinor wave function  $\Phi(z)$  obeys the equation

$$\{\nabla^2 + \kappa_0^2 - 4\pi\hat{v}(z)\} \Phi(z) = 0. \quad (4.7) \quad \{\{\text{EWaveZ2}\}\}$$

In absence of a magnetic field,  $\bar{v}(z)$  is scalar (or proportional to the unit matrix  $\hat{1}$ ), and each spinor component will propagate exactly as in the scalar case of Sec. 2.1. Conversely, if there is a nonzero magnetic field, then the neutron spin will undergo Larmor precession, which in spinor representation shows up as oscillations between the two spinor components. In consequence, when an incident plane wave hits a magnetic medium it becomes a superposition of two plane waves that propagate with two different vertical wavenumbers that correspond to the two eigenvalues of (4.7).

We now consider a homogeneous layer with constant potential. Similar to [55, 56], we write the formal solution of (4.7) as

$$\Phi(z) = e^{-i\hat{\kappa}z} T + e^{i\hat{\kappa}z} R, \quad (4.8) \quad \{\{\text{EWaveZ2}\}\}$$

where  $T$  and  $R$  are the transmitted and reflected spinor amplitudes. By comparison with (4.7), we see that the square of the operator  $\hat{\kappa}$  is

$$\hat{\kappa}^2 = \kappa_0^2 - 4\pi\hat{v} = \kappa_0^2 - 4\pi(\rho^N + \rho^M \check{\mathbf{B}}\hat{\sigma}). \quad (4.9) \quad \{\{\text{Dhp2}\}\}$$

### 4.1.3 Wavenumber operator $\hat{\kappa}$

Without derivation,<sup>1</sup> we state that the square root of  $\hat{\kappa}^2$  is the operator

$$\hat{\kappa} = \frac{1}{2} \left[ (c_+ + c_-) + (c_+ - c_-) \check{\mathbf{B}}\hat{\sigma} \right], \quad (4.10) \quad \{\{\text{Ehp1}\}\}$$

expressed through its eigenvalues

$$c_{\pm} := \sqrt{\kappa_0^2 - 4\pi\rho^N \pm 4\pi\rho^M}. \quad (4.11) \quad \{\{\text{Devp}\}\}$$

With the abbreviations

$$\alpha := c_+ + c_-, \quad \beta := c_+ - c_-, \quad \text{and} \quad \mathbf{b} := \beta\check{\mathbf{B}}, \quad (4.12) \quad \{\{\text{Dabb}\}\}$$

---

<sup>1</sup>To verify, use standard properties of Pauli matrices. Square (4.10) to reproduce (4.9). Then confirm that  $\lambda + \pm^2$  are eigenvalues of  $\hat{\kappa}^2$ . See also [17, § 55, Exercice 1, p. 198].

we obtain the matrix components<sup>2</sup>

$$\hat{\kappa} = \frac{1}{2}(\alpha + \mathbf{b}\hat{\sigma}) = \frac{1}{2} \begin{pmatrix} \alpha + b_z & b_x - ib_y \\ b_x + ib_y & \alpha - b_z \end{pmatrix}. \quad (4.13) \quad \{\text{Dabb}\}$$

For future reference, we note the inverse operator<sup>3</sup>

$$\hat{\kappa}^{-1} = \frac{1}{2c_+c_-} \left[ (c_+ + c_-) - (c_+ - c_-)\check{\mathbf{B}}\hat{\sigma} \right] \quad (4.14) \quad \{\text{Ehpi}\}$$

$$= \frac{2}{\alpha^2 - \beta^2} (a - \mathbf{b}\hat{\sigma}) \quad (4.15) \quad \{\text{Ehpi}\}$$

$$= \frac{2}{\alpha^2 - \beta^2} \begin{pmatrix} \alpha - b_z & -b_x + ib_y \\ -b_x - ib_y & \alpha + b_z \end{pmatrix}. \quad (4.16)$$

It does not exist if  $\rho^N$  is real and  $\rho^M = \kappa_0^2/(4\pi) - \rho^N$ . If  $\rho^M$  is even larger, then  $\hat{\kappa}$  becomes pure imaginary, causing evanescent waves, to be discussed later (Chapter 5).

#### 4.1.4 Eigendecomposition of $\hat{\kappa}$

`{Skeigen}`

To evaluate functions of the operator  $\hat{\kappa}$ , we will need its eigenvalue decomposition. We start with the matrix  $\check{\mathbf{B}}\hat{\sigma}$ , which has the eigenvalues  $\pm 1$  and the normalized eigenspinors

$$V_+ = \frac{1}{\sqrt{2(1 + \check{B}_z)}} \begin{pmatrix} 1 + \check{B}_z \\ \check{B}_x + i\check{B}_y \end{pmatrix}, \quad V_- = \frac{1}{\sqrt{2(1 + \check{B}_z)}} \begin{pmatrix} \check{B}_x - i\check{B}_y \\ -1 - \check{B}_z \end{pmatrix}. \quad (4.17) \quad \{\text{Ev1v2}\}$$

For readability, we have omitted the subscript  $\mathbf{B}$  from the components of  $\check{\mathbf{B}}$ . and the same eigenvectors as  $\check{\mathbf{B}}\hat{\sigma}$ . We introduce the eigenvector matrix

$$\hat{Q}(\mathbf{B}) := (V_+, V_-) = \frac{1}{\sqrt{2(1 + \check{B}_z)}} \begin{pmatrix} 1 + \check{B}_z & \check{B}_x - i\check{B}_y \\ \check{B}_x + i\check{B}_y & -1 - \check{B}_z \end{pmatrix}. \quad (4.18) \quad \{\text{DQofB}\}$$

The normalization factor becomes singular for  $\check{B}_z = -1$ . In this case, the matrix  $\check{\mathbf{B}}\hat{\sigma}$  is just  $\hat{\sigma}_z$  and has eigenvectors  $V_+ = (0, 1)^\dagger$  and  $V_- = (1, 0)^\dagger$ . Furthermore, we need to take care of the case  $\mathbf{B} = 0$ . Altogether, we let

$$\hat{Q}(\mathbf{B}) := \begin{cases} \hat{1} & \text{if } B = 0, \\ \hat{\sigma}_x & \text{if } B_z = -B, \\ (\check{\mathbf{B}} + \check{\mathbf{z}})\hat{\sigma}/\sqrt{2(1 + \check{B}_z)} & \text{else.} \end{cases} \quad (4.19) \quad \{\text{DQofB}\}$$

<sup>2</sup>Currently (jun23) implemented in function `MatrixFlux::computeKappa()`.

<sup>3</sup>Currently (jun23) implemented in function `MatrixFlux::computeInverseKappa()`.

The matrix  $\hat{\kappa}$  has the eigenvalues  $c_{\pm}$ , and the same eigenvectors as  $\check{\mathbf{B}}\hat{\sigma}$ . Accordingly, it has the eigendecomposition

$$\hat{\kappa} = \hat{Q} \begin{pmatrix} c_+ & 0 \\ 0 & c_- \end{pmatrix} \hat{Q}^\dagger, \quad (4.20) \quad \{\{\mathbf{E}\kappa\mathbf{eigen}\}\}$$

and any holomorphic function  $f(\hat{\kappa})$  can be computed as<sup>4</sup>

$$f(\hat{\kappa}) = \hat{Q} \begin{pmatrix} f(c_+) & 0 \\ 0 & f(c_-) \end{pmatrix} \hat{Q}^\dagger. \quad (4.21) \quad \{\{\mathbf{E}f\kappa\mathbf{eigen}\}\}$$

---

<sup>4</sup>Currently (jun23) implemented in function `MatrixFlux::eigenToMatrix`.

## 4.2 Refraction and reflection at interfaces

{Spolif}

### 4.2.1 Transfer matrix

To match solutions at layer interfaces, we use the transfer matrix method introduced in Sec. 2.1.4. That section was formulated in such ways that only minimal modifications are needed now. Instead of the vertical wave function  $\phi(z)$  and the amplitudes  $t$  and  $r$ , we now have the spinors  $\Phi(z)$ ,  $T$ , and  $R$ . Instead of the vertical wavenumber  $\kappa \equiv k_\perp$  (2.6), we have the operator  $\hat{\kappa}$ . The phase factor  $\delta$  (2.29) also becomes an operator,

$$\hat{\delta}_l := e^{i\hat{\kappa}_l d_l}. \quad (4.22) \quad \{\text{\texttt{Dopdel}}\}$$

The equation system (2.32) becomes

$$\begin{pmatrix} T_{l-1} \\ R_{l-1} \end{pmatrix} = \mathbb{M}_l \begin{pmatrix} T_l \\ R_l \end{pmatrix} \quad (4.23) \quad \{\text{\texttt{EcMcP}}\}$$

with the  $4 \times 4$  transfer matrix in place of (2.33)

$$\mathbb{M}_l := \mathbb{D}_{l-1} \mathbb{S}_l. \quad (4.24) \quad \{\text{\texttt{EMDSP}}\}$$

The phase rotation matrix (2.34) is replaced by the block matrix

$$\mathbb{D}_l := \begin{pmatrix} \hat{\delta}_l^{-1} & 0 \\ 0 & \hat{\delta}_l \end{pmatrix}, \quad (4.25) \quad \{\text{\texttt{EMDSP}}\}$$

to be discussed in the next section. The refraction matrix (2.35) also is replaced by a block matrix,

$$\mathbb{S}_l := \frac{1}{2} \begin{pmatrix} \hat{s}_l^+ & \hat{s}_l^- \\ \hat{s}_l^- & \hat{s}_l^+ \end{pmatrix} \quad (4.26) \quad \{\text{\texttt{ESabP}}\}$$

with the coefficients<sup>5</sup>

$$\hat{s}_l \pm := 1 \pm \hat{\kappa}_{l-1}^{-1} \hat{\kappa}_l. \quad (4.27) \quad \{\text{\texttt{ESabP}}\}$$

### 4.2.2 Phase rotation matrix

{Sphase}

With the eigendecomposition (4.21), the phase rotation matrix (4.22) can be written<sup>6</sup>

$$\hat{\delta} = e^{i\hat{\kappa}d} = \hat{Q} \begin{pmatrix} e^{id\kappa_+} & 0 \\ 0 & e^{id\kappa_-} \end{pmatrix} \hat{Q}^\dagger. \quad (4.28) \quad \{\text{\texttt{EdP2}}\}$$

For the analysis of numerical stability, the critical factor  $e^{i\alpha d/2}$  may be drawn in front of  $\hat{Q}$  in (4.28),

$$\hat{\delta} = e^{i\alpha d/2} \hat{Q} \begin{pmatrix} e^{id\beta/2} & 0 \\ 0 & e^{-id\beta/2} \end{pmatrix} \hat{Q}^\dagger. \quad (4.29) \quad \{\text{\texttt{EdP2a}}\}$$

<sup>5</sup>Currently (jun23), the matrix blocks  $\hat{s}_l^+$  and  $\hat{s}_l^-$ , possibly modified by roughness factors (see below .... TODO), are computed through local function `refractionMatrixBlocks` in `ComputeFluxMagnetic.cpp`.

<sup>6</sup>Currently (jun23) implemented in local function `PhaseRotationMatrix` in file `MatrixFlux.cpp`.

## 4.3 From old document “PolarizedImplementation”

### 4.3.1 Numerically stable implementation

{sec:implementation}

We combine the amplitude vectors for  $+$  and  $-$  polarization into a single matrix of dimension  $4 \times 2$

$$\begin{pmatrix} \underline{\underline{T_j}} \\ \underline{\underline{R_j}} \end{pmatrix} = \begin{pmatrix} \underline{t_j^+} & \underline{t_j^-} \\ \underline{r_j^+} & \underline{r_j^-} \end{pmatrix}, \quad (4.30)$$

where the submatrices

$$\underline{\underline{T_j}} = \begin{pmatrix} \underline{t_j^+}, \underline{t_j^-} \end{pmatrix} \quad \text{and} \quad \underline{\underline{R_j}} = \begin{pmatrix} \underline{r_j^+}, \underline{r_j^-} \end{pmatrix} \quad (4.31)$$

are of dimension  $2 \times 2$ . The transfer matrix equation (4.23) can then be written simultaneously for both polarization states as

$$\begin{pmatrix} \underline{\underline{T_a}} \\ \underline{\underline{R_a}} \end{pmatrix} = \mathbb{M}_{ab} \begin{pmatrix} \underline{\underline{T_b}} \\ \underline{\underline{R_b}} \end{pmatrix}. \quad (4.32)$$

Explicitly performing this multiplication yields two matrix recursion equations

$$\underline{\underline{T_a}} = \frac{1}{2} \hat{\delta}^{-1} \left( \hat{s}^+ \underline{\underline{T_b}} + \hat{s}^- \underline{\underline{R_b}} \right) \quad (4.33)$$

$$\underline{\underline{R_a}} = \frac{1}{2} \hat{\delta} \left( \hat{s}^- \underline{\underline{T_b}} + \hat{s}^+ \underline{\underline{R_b}} \right) \quad (4.34)$$

After every step (4.23), we want to rotate and normalize the polarization, such that we obtain the bottom boundary condition  $\underline{\underline{T_a}} = \underline{\underline{1}}$ . For this purpose, we define the rotation matrix  $\underline{\underline{S}}$  as

$$\underline{\underline{T_a'}} = \underline{\underline{T_a}} \cdot \underline{\underline{S_a}} = \underline{\underline{1}}, \quad (4.35)$$

and it must also be applied to rotate the reflected components as well <sup>7</sup>

$$\underline{\underline{R_a'}} = \underline{\underline{R_a}} \cdot \underline{\underline{S_a}}. \quad (4.36)$$

Consequently, the recursion equations reduce to the primed version

{eq:primed\_recursion}

$$\underline{\underline{T_a'}} = \underline{\underline{1}} \quad (4.37a)$$

$$\underline{\underline{S_a}}^{-1} = \frac{1}{2} \hat{\delta}^{-1} \left( \hat{s}^+ + \hat{s}^- \underline{\underline{R_b'}} \right) =: \hat{\delta}^{-1} \cdot \tilde{\underline{\underline{S_a}}}^{-1} \quad (4.37b)$$

$$\underline{\underline{R_a'}} = \frac{1}{2} \hat{\delta} \left( \hat{s}^- + \hat{s}^+ \underline{\underline{R_b'}} \right) \cdot \underline{\underline{S_a}}. \quad (4.37c)$$

---

<sup>7</sup>What happens here is a rotation of the wave function written as a superposition  $\underline{\Phi_a'}^\pm = a^\pm \underline{\Phi_a}^+ + b^\pm \underline{\Phi_a}^-$ . This is just written as a single matrix equation and from this it is obvious that the same matrix must be applied to both  $\underline{\underline{T_a}}$  and  $\underline{\underline{R_a}}$ .

This process requires the inverse of  $\underline{\underline{S}}_a^{-1}$ , which is easy to obtain

$$\underline{\underline{S}}_a = \frac{1}{\det \underline{\underline{\tilde{S}}}_a^{-1}} \begin{pmatrix} \left( \underline{\underline{\tilde{S}}}_a^{-1} \right)_{1,1} & - \left( \underline{\underline{\tilde{S}}}_a^{-1} \right)_{1,0} \\ - \left( \underline{\underline{\tilde{S}}}_a^{-1} \right)_{0,1} & \left( \underline{\underline{\tilde{S}}}_a^{-1} \right)_{0,0} \end{pmatrix} \hat{\delta}, \quad (4.38)$$

and since it does not contain the inverse  $\delta^{-1}$ -matrix anymore can be evaluated numerically stable.

For the computation of reflectivity alone, we would be done at this point, however, for perturbation theory, we still need the amplitudes within the layer stack. Therefore, all rotations of the polarization need to be forward-propagated according to

$$\underline{\underline{T}}_a = \prod_{i=m-1}^0 \underline{\underline{S}}_i \quad (4.39)$$

$$\underline{\underline{R}}_a = \underline{\underline{R}}'_a \cdot \prod_{i=m-1}^0 \underline{\underline{S}}_i \quad (4.40)$$

$$\text{for } a \geq 1, \text{ where } \prod_{i=m-1}^0 \underline{\underline{S}}_i = \underline{\underline{S}}_{a-1} \underline{\underline{S}}_{a-2} \cdots \underline{\underline{S}}_0 \quad (4.41)$$

The proof of these relations can be done as follows. In order to obtain the correct amplitudes in each layer, after every step of the recursion (4.37) the applied rotation needs to be propagated down through the bottom of the stack according to

$$\text{for } m = N - 1 \dots 0 \quad \text{outer iteration from bottom to top} \quad (4.42)$$

$$\underline{\underline{T}}'_m = \underline{\underline{1}} \quad (4.43)$$

$$\underline{\underline{R}}'_m = \underline{\underline{R}}_m \cdot \underline{\underline{S}}_m \quad (4.44)$$

$$\text{for } i = m + 1 \dots N \quad (4.45)$$

$$\underline{\underline{T}}_i = \underline{\underline{T}}_i \cdot \underline{\underline{S}}_m \quad (4.46)$$

$$\underline{\underline{R}}_i = \underline{\underline{R}}_i \cdot \underline{\underline{S}}_m \quad (4.47)$$

**Remark** The defined  $\underline{\underline{R}}'_m$  is equal to the  $\underline{\underline{X}}_m$  in the Parratt formalism, and equation (4.37)c is almost identical to the usual recursion in  $\underline{\underline{X}}_m$  [56, 55], apart from the treatment of the phase factor. The second recursion equation in [56, 55] that yields the amplitudes is replaced by storing the intermediate  $\underline{\underline{S}}_m$ .

### 4.3.2 Roughness

For a detailed description of the implemented roughness models, we refer to the document *Refraction, reflection, and scattering from rough interfaces* in theory/Roughness.pdf.

#### 4.3.2.1 Tanh Profile

As in the scalar implementation, the analytical tanh interface profile is implemented by replacing the Fresnel reflection and transmission coefficients in the transfer matrix

$$\underline{\underline{S}}_{ab} = \begin{pmatrix} 1 + \underline{\underline{P}}_{ab} & 1 - \underline{\underline{P}}_{ab} \\ 1 - \underline{\underline{P}}_{ab} & 1 + \underline{\underline{P}}_{ab} \end{pmatrix} \quad (4.48)$$

to incorporate the analytical solution of the Helmholtz equation via

$$\underline{\underline{S}}_{ab} = \begin{pmatrix} 1/\underline{\underline{\mathcal{R}}}_{ab} + \underline{\underline{P}}_{ab}\underline{\underline{\mathcal{R}}}_{ab} & 1/\underline{\underline{\mathcal{R}}}_{ab} - \underline{\underline{P}}_{ab}\underline{\underline{\mathcal{R}}}_{ab} \\ 1/\underline{\underline{\mathcal{R}}}_{ab} - \underline{\underline{P}}_{ab}\underline{\underline{\mathcal{R}}}_{ab} & 1/\underline{\underline{\mathcal{R}}}_{ab} + \underline{\underline{P}}_{ab}\underline{\underline{\mathcal{R}}}_{ab} \end{pmatrix}. \quad (4.49)$$

Here, the roughness correction factor  $\underline{\underline{\mathcal{R}}}_{ab}$  is also a  $2 \times 2$  matrix and is given by

$$\underline{\underline{\mathcal{R}}}_{ab} = \frac{\sqrt{\tanhc\left\{(\pi/2)^{3/2} \underline{\underline{\sigma}}_a \underline{\underline{p}}_b\right\}}}{\sqrt{\tanhc\left\{(\pi/2)^{3/2} \underline{\underline{\sigma}}_a \underline{\underline{p}}_a\right\}}} = \underline{\underline{\mathcal{R}}}_b \cdot \underline{\underline{\mathcal{R}}}_a^{-1} \quad (4.50)$$

This expression is evaluated via the eigenvalue decomposition

$$\underline{\underline{\mathcal{R}}}_b = \underline{\underline{Q}}_b \begin{pmatrix} \sqrt{\tanhc\left(\underline{\underline{\sigma}}'_a \lambda_+^b\right)} & 0 \\ 0 & \sqrt{\tanhc\left(\underline{\underline{\sigma}}'_a \lambda_-^b\right)} \end{pmatrix} \underline{\underline{Q}}_b^\dagger \quad (4.51) \quad \{\text{eq:roughness\_tanh\_eigen}\}$$

$$\underline{\underline{\mathcal{R}}}_a^{-1} = \underline{\underline{Q}}_a \begin{pmatrix} \frac{1}{\sqrt{\tanhc\left(\underline{\underline{\sigma}}'_a \lambda_+^a\right)}} & 0 \\ 0 & \frac{1}{\sqrt{\tanhc\left(\underline{\underline{\sigma}}'_a \lambda_-^a\right)}} \end{pmatrix} \underline{\underline{Q}}_a^\dagger, \quad (4.52) \quad \{\text{eq:roughness\_tanh\_eigen}\}$$

where we have defined  $\underline{\underline{\sigma}}'_a = (\pi/2)^{3/2} \underline{\underline{\sigma}}_a$  and the transformation matrix  $\underline{\underline{Q}}$  is the same as in equation (4.19).

The case of zero magnetic field  $\vec{e}_b = 0$  needs to be treated separately again, in that case we have

$$\underline{\underline{\mathcal{R}}}_b = \begin{pmatrix} \sqrt{\tanhc\left(1/2 \underline{\underline{\sigma}}'_a \alpha_b\right)} & 0 \\ 0 & \sqrt{\tanhc\left(1/2 \underline{\underline{\sigma}}'_a \alpha_b\right)} \end{pmatrix} \quad (4.53)$$

$$\underline{\underline{\mathcal{R}}}_a^{-1} = \begin{pmatrix} \frac{1}{\sqrt{\tanhc\left(1/2 \underline{\underline{\sigma}}'_a \alpha_a\right)}} & 0 \\ 0 & \frac{1}{\sqrt{\tanhc\left(1/2 \underline{\underline{\sigma}}'_a \alpha_a\right)}} \end{pmatrix} \quad (4.54)$$



#### 4.3.2.2 Névot-Croce

The interface transition part of the transfer matrix is replaced with the expression

$$\underline{\underline{S}}_{ab} = \frac{1}{2} \begin{pmatrix} (1 + \underline{\underline{P}}) \exp - \left( \underline{\underline{p}}_b - \underline{\underline{p}}_a \right)^2 \frac{\underline{\underline{\sigma}}_a^2}{2} & (1 - \underline{\underline{P}}) \exp - \left( \underline{\underline{p}}_b + \underline{\underline{p}}_a \right)^2 \frac{\underline{\underline{\sigma}}_a^2}{2} \\ (1 - \underline{\underline{P}}) \exp - \left( \underline{\underline{p}}_b + \underline{\underline{p}}_a \right)^2 \frac{\underline{\underline{\sigma}}_a^2}{2} & (1 + \underline{\underline{P}}) \exp - \left( \underline{\underline{p}}_b - \underline{\underline{p}}_a \right)^2 \frac{\underline{\underline{\sigma}}_a^2}{2} \end{pmatrix}, \quad (4.55) \quad \{\text{eq:transfer\_matrix\_Giba}\}$$

that is the polarized equivalent of the scalar implementation. For brevity the indices on the  $\underline{\underline{P}}_{ab}$  matrices are omitted in this section. In order to evaluate this matrix, we need to compute the exponential of a matrix of the form

$$\underline{\underline{P}}_{ab} = \left( \underline{\underline{p}}_b \pm \underline{\underline{p}}_a \right)^2. \quad (4.56)$$

This matrix can be rewritten as

$$\underline{\underline{P}}_{ab} = \underline{\underline{p}}_b \pm \underline{\underline{p}}_a \quad (4.57)$$

$$= \frac{1}{2} \left[ \alpha_b \pm \alpha_a + \hat{\boldsymbol{\sigma}} \cdot \underbrace{\left( \beta_b \vec{b}_b \pm \beta_a \vec{b}_a \right)}_{:= \vec{b}'} \right]. \quad (4.58)$$

Now the vector  $\vec{b}'$  is a complex vector, that will be normalized according to

$$\vec{b}'' = \frac{\vec{b}'}{\vec{b}'^T \cdot \vec{b}'}, \quad (4.59)$$

and we have the new eigenvalue

$$\beta_{ab} = \vec{b}'^T \cdot \vec{b}'. \quad (4.60)$$

It must be noted, that this normalization is not based on the usual inner product with a complex conjugate, but really only the squared elements of the vector. This is due to the fact that the  $p$ -matrix is only squared and not conjugated. The vectors  $\vec{b}'$  and  $\vec{b}''$  should carry a  $\pm$ , depending on which matrix is being evaluated, however, for clarity we drop this sign. Consequently, we can now write the resulting matrix

$$\underline{\underline{P}}_{ab} = \frac{1}{2} \left( \alpha_{ab} + \beta_{ab} \hat{\boldsymbol{\sigma}} \cdot \vec{b}'' \right), \quad (4.61)$$

with  $\alpha_{ab} = \alpha_b \pm \alpha_a$ . This expression can easily be squared

$$\underline{\underline{P}}_{ab}^2 = \frac{1}{4} \left( \alpha_{ab}^2 + \beta_{ab}^2 + 2\alpha_{ab}\beta_{ab}\hat{\boldsymbol{\sigma}} \cdot \vec{b}'' \right) \quad (4.62)$$

$$= \frac{1}{4} \left( \alpha''_{\underline{\underline{1}}} + \beta'' \hat{\boldsymbol{\sigma}} \cdot \vec{b}'' \right). \quad (4.63)$$

The exponential of this can now be computed using the well-known eigendecomposition of the second term. The eigenvalues are now  $\pm\beta''$  and the corresponding eigenvectors are given by

$$\underline{v}_1 = \frac{1}{\sqrt{2(b_z'' + 1)}} \begin{pmatrix} 1 + b_z'' \\ b_x'' + ib_y'' \end{pmatrix} \quad \underline{v}_2 = \frac{1}{\sqrt{2(1 - b_z'')}} \begin{pmatrix} b_z'' - 1 \\ b_x'' + ib_y'' \end{pmatrix}, \quad (4.64)$$

such that we have the usual eigenvalue equation  $\hat{Q}\underline{v}_n = \beta''\underline{v}_n$  with  $\hat{Q} = (\underline{v}_1, \underline{v}_2)$ . The inverse  $\hat{Q}^{-1}$  is given by

$$\hat{Q}^{-1} = \begin{pmatrix} \underline{v}_1'^T \\ \underline{v}_2'^T \end{pmatrix}, \quad (4.65)$$

where

$$\underline{v}_1' = \frac{1}{\sqrt{2(b_z'' + 1)}} \begin{pmatrix} 1 + b_z'' \\ b_x'' - ib_y'' \end{pmatrix} \quad \underline{v}_2' = \frac{1}{\sqrt{2(1 - b_z'')}} \begin{pmatrix} b_z'' - 1 \\ b_x'' - ib_y'' \end{pmatrix}. \quad (4.66)$$

Putting this all together, we obtain for  $\vec{b}'' \neq 0$

$$\exp - \left( \underline{p}_b - \underline{p}_a \right)^2 \underline{\sigma}_b^2 / 2 = \begin{pmatrix} \exp \alpha'' & 0 \\ 0 & \exp \alpha'' \end{pmatrix} \cdot \hat{Q} \cdot \begin{pmatrix} \exp \beta'' & 0 \\ 0 & \exp -\beta'' \end{pmatrix} \hat{Q}^{-1} \quad (4.67)$$

and for  $\vec{b}'' = 0$

$$\exp - \left( \underline{p}_b - \underline{p}_a \right)^2 \sigma_b^2 / 2 = \begin{pmatrix} \exp \alpha'' & 0 \\ 0 & \exp \alpha'' \end{pmatrix}. \quad (4.68)$$

For brevity, the factor  $\underline{\sigma}_b^2/2$  was neglected in  $\alpha''$  and  $\beta''$ .

### 4.3.3 Reflection matrix and boundary conditions

In the current formalism, the reflection operator is directly computed by the implemented iterative method and given by  $\underline{R}_0$ . In order to start the backwards iteration described in Section 4.3.1, one needs to impose the bottom boundary condition of no reflected wave, i.e.  $\underline{R}_N = \underline{0}$ . Furthermore, the iteration starts with pure polarization states, i.e.  $\underline{T}_N = \underline{1}$ , that is subsequently rotated to the final transmitted polarization state, by applying the top boundary condition  $\underline{T}_0 = \underline{1}$ .

#### 4.3.4 Amplitudes for DWBA computations

The DWBA computations require all four amplitudes that belong to the 4 waves traveling with different wave vectors separately. This requires the decomposition of

$$\underline{\Phi}_j(z) = \exp i \underline{p}_a(z - z_{j-1}) \underline{t}_j + \exp -i \underline{p}_a(z - z_{j-1}) \underline{r}_j, \quad (4.69)$$

into its eigenmodes. In order to achieve this, we again apply the eigenvalue decomposition of  $\underline{p}_a$ , as it is also used in (4.51), where the transformation matrix is given by ?? and the eigenvalues are of course  $c_+$  and  $c_-$  and we have

$$\exp i \underline{p}_j z = \hat{Q} \cdot \exp i \Lambda z \cdot \hat{Q}^\dagger \quad (4.70)$$

$$= \hat{Q} \cdot \begin{pmatrix} \exp i c_+ z & 0 \\ 0 & 0 \end{pmatrix} \cdot \hat{Q}^\dagger + \hat{Q} \cdot \begin{pmatrix} 0 & 0 \\ 0 & \exp i c_- z \end{pmatrix} \cdot \hat{Q}^\dagger \quad (4.71)$$

$$= \exp i c_+ z \hat{Q} \cdot \begin{pmatrix} 1 & 0 \\ 0 & 0 \end{pmatrix} \cdot \hat{Q}^\dagger + \exp i c_- z \hat{Q} \cdot \begin{pmatrix} 0 & 0 \\ 0 & 1 \end{pmatrix} \cdot \hat{Q}^\dagger. \quad (4.72)$$

This decomposition is valid unless the magnetic field vanishes. In the latter case, we have

$$\exp i \underline{p}_a z = \exp i c_+ z \cdot \begin{pmatrix} 1 & 0 \\ 0 & 0 \end{pmatrix} + \exp i c_- z \cdot \begin{pmatrix} 0 & 0 \\ 0 & 1 \end{pmatrix}. \quad (4.73)$$

The resulting matrix can be written as a sum of two matrices

$$\exp i \underline{p}_a z = \exp i c_+ z \underline{T}_2 + \exp i c_- z \underline{T}_1, \quad (4.74)$$

and the needed amplitudes are then given by

$$\underline{T}_1^+ = \underline{T}_1 \cdot \underline{t} \quad \underline{R}_1^+ = \underline{T}_1 \cdot \underline{r} \quad \dots \quad (4.75)$$

The matrices  $\underline{T}_1$  and  $\underline{T}_2$  are computed via `MatrixRTCoefficients::T1Matrix` and `MatrixRTCoefficients::T2Matrix`.

These vector amplitudes  $\underline{T}_1^+$  etc. are computed in `MatrixRTCoefficients::T1plus` etc.

#### 4.3.5 Limiting case $\kappa \rightarrow 0$

This case is implemented in the same way as for the scalar case, that is described in Sec. 2.2.2 of the BornAgain manual version 1.7.2. For clarity, we briefly summarize the treatment here.

- One single layer: This is a trivial case, nothing needs to be calculated here as the outgoing wave is equal to the incoming one. As a consequence, it means that we have  $\underline{T}_0 = \underline{1}$  and  $\underline{R}_0 = 0$

- More than one layer: In that case the limit  $\kappa \rightarrow 0$  is well defined. For  $\kappa = 0$ , we have  $\underline{\underline{R_0}} = -\underline{\underline{T_0}} = -\underline{\underline{1}}$  and  $\underline{\underline{T_j}} = \underline{\underline{R_j}} = 0$  for  $j > 0$ .
- $\kappa = 0$  in intermediate layer: This case is not treated separately but automatically covered by the solution also present for scalar computations. In `KzComputation::checkForUnderflow` a tiny imaginary part is added if the resulting value for  $\kappa^2$  is getting very small.

For a single layer, the correct computation of these conditions is checked in `SpecularMagneticTest::test_degenera`

#### 4.3.6 Test suite

The scalar amplitudes allow the computation of vector amplitudes according to

$$\begin{array}{llll} \underline{\underline{T_1^+}} = 0 & \underline{\underline{T_2^+}} = \begin{pmatrix} t \\ 0 \end{pmatrix} & \underline{\underline{T_1^-}} = \begin{pmatrix} 0 \\ t \end{pmatrix} & \underline{\underline{T_2^-}} = 0 \\ \underline{\underline{R_1^+}} = 0 & \underline{\underline{R_2^+}} = \begin{pmatrix} r \\ 0 \end{pmatrix} & \underline{\underline{R_1^-}} = \begin{pmatrix} 0 \\ r \end{pmatrix} & \underline{\underline{R_2^-}} = 0 \end{array}$$

These relations allow to compare the amplitudes from a scalar computation to a polarized result, in case there is no magnetization present. For two layers, consistency between the scalar and polarized computation is checked in `SpecularMagneticTest::testZeroField`

#### 4.3.7 Magnetic field in BornAgain

The z-component is afaik currently explicitly set conserved.

Imo this is bit funny, as Dmitry also remarked in [Issue 2417](#)

##### 4.3.7.1 Magnetic field in the fronting medium

As previously described in [57], it is reasonable to assume that the incoming beam penetrates the fronting medium of the sample assembly from a side. This results in  $k_z$  being preserved even when there is a non-zero magnetic field in the fronting medium. To account for that in the calculations, one needs to replace  $k_{0z}^2$  with  $k_{0z}^2 + 4\pi\check{\rho}_{front}$  in equation ??, with  $\check{\rho}_{front}$  being the SLD matrix for the fronting medium. It is also equivalent to subtracting the magnetic field of the fronting medium,  $\mathbf{B}_{front}$ , from the magnetic field of each layer, thus amending  $\check{\rho}_M$ :

$$\check{\rho}'_M = -\frac{m}{2\pi\hbar^2}\check{\boldsymbol{\mu}}(\mathbf{B} - \mathbf{B}_{front}).$$

This amendment also concerns the nuclear (non-magnetic) scattering length density:

$$\rho'_n = \rho_n - \rho_{n,front},$$

where  $\rho_{n,front}$  is the nuclear SLD of the fronting medium.

TODO: Check this in the code

Further in the text we will omit the primes and handling of the fronting medium's properties, however, implying that both magnetic fields and nuclear SLDs are amended in the way mentioned above.

#### 4.3.7.2 Magnetic field $z$ -component conservation

In the framework of the problem, the sample is assumed to be infinite along the  $x$  and  $y$  axes, all parameters being constant inside each layer. This is equivalent to the requirement of translational invariance along these axes. On the other hand, magnetic field is known to be divergence-free,

$$\nabla \cdot \mathbf{B} = 0.$$

Both of these conditions result in the  $z$ -component of the magnetic field (that is, the component normal to the sample surface),  $B_z$ , being preserved in the whole sample and fronting medium:

$$\frac{\partial B_z}{\partial z} \equiv 0.$$

#### 4.3.8 Intensity and density matrix

{sec:intensity\_analysis}

The wave function in the ambient material is given by

$$\underline{\Phi}_0(z) = \underbrace{\exp ip_0 t_0}_{\underline{\Phi}_i(z)} + \underbrace{\exp -ip_0 r_0}_{\underline{\Phi}_r(z)}. \quad (4.76)$$

Here  $\underline{\Phi}_i$  is the incoming wave in a given polarization state  $\underline{t}_0$  and  $\underline{\Phi}_r$  is the reflected wave. The intensity measured on a detector is without polarization analysis given by

$$I_R = |\underline{\Phi}_r|^2 = \langle \underline{\Phi}_r | \underline{\Phi}_r \rangle \quad (4.77) \quad \{\text{eq:intensity\_no\_polariz}\}$$

This would allow for the direct computation of the reflected intensity if  $\underline{t}_0$  would describe the incoming polarization state. In case of an arbitrary but pure state of the incoming beam, the reflected wave can be described by a reflection matrix

$$\underline{\Phi}_r(z) = \underline{\mathcal{R}} \underline{\Phi}_i(z), \quad (4.78) \quad \{\text{eq:intensity\_no\_polariza}\}$$

where  $\underline{\mathcal{R}}$  is a  $2 \times 2$  matrix:

$$\underline{\mathcal{R}} = \begin{pmatrix} r_{++} & r_{-+} \\ r_{+-} & r_{--} \end{pmatrix} \quad (4.79)$$

with its non-diagonal elements contributing to spin-flip reflections. If we consider the intensities right at the topmost interface of the sample at  $z = z_0 = 0$ , the phase factors drop out and we find the relation

$$\underline{r}_0 = \underline{\mathcal{R}} \underline{t}_0. \quad (4.80) \quad \{\text{eq:R-matrix}\}$$

Therefore, as soon as  $\underline{\mathcal{R}}$  is known, it is trivial to perform a calculation for any desired incoming polarization state. It is clear that (4.80) is a system of two equations with four unknown variables. Hence if two pairs of incoming and reflected waves  $\underline{t}_0, \underline{r}_0$  and  $\underline{t}'_0, \underline{r}'_0$

are known, the reflection matrix can be determined (if they are linearly independent). Writing these four equations as a matrix

$$(\underline{r}_0, \underline{r}_0') = \underline{\mathcal{R}} (\underline{t}_0, \underline{t}_0') , \quad (4.81) \quad \{\{\text{eq:R-matrix2}\}\}$$

one can see that the inversion of this equation becomes trivial if the two incoming waves are chosen such that they are in a  $+$  and  $-$  polarization state. If they are chosen differently, inverting equation (4.81) corresponds to the rotation of the incoming polarization vectors such that they become pure  $+$  and  $-$  waves.

If we perform polarization analysis, the analyzer will only pass a wave in the  $\Phi_f$  polarization state. Hence the reflected wave needs to be projected onto this state to obtain the measured intensity

$$I_R = \left| \langle \Phi_f | \underline{\mathcal{R}} | \Phi_i \rangle \right|^2 = \langle \Phi_f | \underline{\mathcal{R}} | \Phi_i \rangle \cdot \langle \Phi_i | \underline{\mathcal{R}}^\dagger | \Phi_f \rangle . \quad (4.82) \quad \{\{\text{eq:intensity_polarizati}\}\}$$

Following [58], we introduce the density matrix  $\underline{f}_p$  (polarizer) for an arbitrary mixed state of incoming beam and, correspondingly,  $\underline{f}_a$  (analyzer) for an arbitrary mixed state passed through a polarization analyzer:

$$\underline{f}_p = \frac{1}{2} (\underline{1} + \hat{\sigma} \cdot \underline{p}) \quad \underline{f}_a = \frac{1}{2} (\underline{1} + \hat{\sigma} \cdot \underline{a}) . \quad (4.83) \quad \{\{\text{eq:density_operators}\}\}$$

The beam polarization as well as analyzer direction and efficiency are described by the Bloch vectors  $\underline{p}, \underline{a} \in \mathbb{R}^3$ .  $|\underline{p}| = 1$  corresponds to some pure state of beam polarization, while  $|\underline{p}| < 1$  is for a state mixture (partial polarization). The same holds for non-perfect analyzers, where we call  $|\underline{p}|$  the efficiency.<sup>8</sup>

In order to compute the reflection coefficient for a mixed-state beam, equation (4.82) needs to be rewritten in the density matrix formalism

$$\langle \Phi_i | \underline{\mathcal{R}}^\dagger | \Psi_f \rangle \cdot \langle \Phi_f | \underline{\mathcal{R}} | \Phi_i \rangle = \text{Tr} \left( |\Phi_i\rangle \langle \Phi_i| \underline{\mathcal{R}}^\dagger |\Phi_f\rangle \langle \Phi_f| \underline{\mathcal{R}} \right) . \quad (4.84) \quad \{\{\text{eq:intensity_trace}\}\}$$

Here  $\text{Tr}$  denotes trace operation.  $|\Phi_f\rangle \langle \Phi_f|$  and  $|\Phi_i\rangle \langle \Phi_i|$  are respective outer products for the  $\Phi_f$  and  $\Phi_i$  pure states and coincide with the corresponding density matrices. To generalize expression (4.84) to mixed states of the incoming beam and polarization analyzer, one has to replace the explicit outer products with the density matrices  $\underline{f}_p, \underline{f}_a$  that describe the polarizer and analyzer as defined in (4.83). This will automatically take into account the averaging over all possible initial and final pure states of the system. Therefore, the final expression for  $I_R$  reads

$$I_R = \text{Tr} \left( \underline{f}_p \underline{\mathcal{R}}^\dagger \underline{f}_a \underline{\mathcal{R}} \right) . \quad (4.85) \quad \{\{\text{eq:32}\}\}$$

This expression should work for both a perfect and imperfect polarizer and analyzer. It also seems to be consistent with Wildes [59, 60], this paper was recommended as standard reference on this topic by Artur.

---

<sup>8</sup>In PolarizedSpecular, Sec. 5.1, Dmitry claims this treatment of a non-perfect analyzer is not possible and suggests a different treatment. However i (rb) think that his argument is not correct.

It needs to be noted that the limit  $|\vec{a}| = 0$  does not correspond to no polarization analysis (i.e. a very common experiment without polarization analysis). Instead, if no polarization analysis is performed, writing (4.77) in the density matrix formalism yields

$$I_R = |\underline{\Phi}_r|^2 = \left\langle \underline{\Phi}_i \left| \underline{\mathcal{R}}^\dagger \underline{\mathcal{R}} \right| \underline{\Phi}_i \right\rangle = \text{Tr} \left( \underline{\underline{f_p}} \underline{\mathcal{R}}^\dagger \underline{\mathcal{R}} \right) , \quad (4.86) \quad \{\text{eq:32}\}$$

which corresponds to  $\underline{\underline{f_a}} = \underline{\underline{1}}$ .

TODO: can we show the equivalence between the Wildes approach and our density matrix formulas?

## 4.4 From old document “Reflectivity”

### 4.4.1 Parratt formalism

$$X_m = \hat{r}_m \hat{t}_m^{-1} \quad (4.87)$$

$$X_m = \exp ip_m d_m \tilde{X}_m \exp ip_m d_m \quad (4.88)$$

$$\tilde{X}_m = \frac{1 - p_m^{-1} p_{m+1} + (1 + p_m^{-1} p_{m+1}) X_{m+1}}{1 + p_m^{-1} p_{m+1} + (1 - p_m^{-1} p_{m+1}) X_{m+1}} \quad (4.89)$$

$$t_{m+1} = \frac{(1 + \tilde{X}_m) \exp ip_m d_m}{1 + X_{m+1}} t_m \quad (4.90)$$

- Kentzinger et al. introduce structural (nuclear) roughness into this formalism by adding Nevôt-Croce factors to the operator  $(1 - p_m^{-1} p_{m+1})$
- [55] mention the numerical stability of this algorithm due to the strictly positive imaginary parts in the phase factors
- Here  $X_m$  is a  $2 \times 2$  operator



## 4.5 From old document “Stratified”

### 4.5.1 The split boundary problem

{SsplibouP}

A numerically stable recursive solution of the split boundary problem for polarized radiation has been proposed in [13], and summarized in notation closer to ours in [14]. Their argument can be further simplified as follows.

SCALAR CASE:

We consider layers  $a, b := a + 1, \nu$ . The transfer matrix (2.46) obeys the recursion

$$M_{a\nu} = M_{ab} M_{b\nu}. \quad (4.91)$$

With the conversion functions (2.48) and (2.49), we can derive a recursion for  $W$ :

$$W_{a\nu} = \mathcal{W}(M_{ab} \mathcal{M}(W_{b\nu})). \quad (4.92) \quad \{\{EWrecu\}\}$$

The per-layer transfer matrices  $M_{ab}$  are given; the  $W_{a\nu}$  shall be determined for  $a$  from  $\nu - 1$  to 0.

Once we have  $W_{0\nu}$ , we can use

$$\begin{pmatrix} t_\nu \\ r_0 \end{pmatrix} = W_{0\nu} \begin{pmatrix} 1 \\ 0 \end{pmatrix} \quad (4.93) \quad \{\{Ert\_backward\}\}$$

to compute the reflected amplitude  $r_0$  in the top (air/vacuum) layer. This backward computation must then be followed by a forward computation of

$$\begin{pmatrix} t_a \\ r_a \end{pmatrix} = M_{0a}^{-1} \begin{pmatrix} 1 \\ r_0 \end{pmatrix}. \quad (4.94) \quad \{\{Ert\_forward\}\}$$

THE FOLLOWING WAS OUTCOMMENTED:

However, determining the  $W_{a\nu}$  is not a goal in itself; we shall only evaluate them insofar as needed for computing Ultimately, we want to apply (4.95) to layers  $i = 0, f = \nu$ , with  $\underline{r}_\nu = 0$ . Therefore, we only need to derive the  $tt$  and  $rt$  components of  $W_{0\nu}$ , whereas the  $tr$  and  $rr$  components are irrelevant. It turns out that this also holds for the inner terms of the recursion (4.92): we only need the  $tt$  and  $rt$  components of the intermediate  $W_{0a}$ .

NOW THE POLARIZED CASE

THE FOLLOWING WAS OUTCOMMENTED:

The homogeneous linear equation (4.23) can be reorganized as

$$\begin{pmatrix} \underline{t}_f \\ \underline{r}_i \end{pmatrix} = \mathbb{W}_{if} \begin{pmatrix} \underline{t}_i \\ \underline{r}_f \end{pmatrix} \quad (4.95) \quad \{\{EcWcP\}\}$$

for whatever layers  $j, k$ . Following [14], we write matrix components as

$$\mathbb{W} =: \begin{pmatrix} \underline{\underline{W}}^{tt} & \underline{\underline{W}}^{tr} \\ \underline{\underline{W}}^{rt} & \underline{\underline{W}}^{rr} \end{pmatrix}, \quad (4.96) \quad \{\{EcWcP\}\}$$

and similarly for matrix  $\mathbb{M}$  of (4.23). Combining (4.23) and (4.95), we can express  $\mathbb{W}$  as function of  $\mathbb{M}$ ,

$$\mathbb{W}(\mathbb{M}) = \begin{pmatrix} \underline{\underline{M}}^{tt-1} & \underline{\underline{M}}^{tt-1} \underline{\underline{M}}^{tr} \\ \underline{\underline{M}}^{rt} \underline{\underline{M}}^{tt-1} & (\underline{\underline{M}}^{rr} - \underline{\underline{M}}^{rt} \underline{\underline{M}}^{tt-1} \underline{\underline{M}}^{tr}) \end{pmatrix}, \quad (4.97) \quad \{\{\text{EM2Wpol}\}\}$$

and conversely,  $\mathbb{M}$  as function of  $\mathbb{W}$

$$\mathbb{M}(\mathbb{W}) = ?? . \quad (4.98) \quad \{\{\text{EW2Mpol}\}\}$$

Now consider layers 0,  $a$ ,  $b := a + 1$ . The transfer matrix obeys the recursion

$$\mathbb{M}_{0b} = \mathbb{M}_{0a} \mathbb{M}_{ab}. \quad (4.99) \quad \{\{\text{EW2Mpol}\}\}$$

With the conversions (4.97) and (4.98), we can derive a recursion for  $\mathbb{W}$ :

$$\mathbb{W}_{0b} = \mathbb{W}(\mathbb{M}(\mathbb{W}_{0a}) \mathbb{M}_{ab}). \quad (4.100) \quad \{\{\text{EWrecupo}\}\}$$

Ultimately, we want to apply (4.95) to layers  $i = 0$ ,  $f = \nu$ , with  $\underline{r}_\nu = 0$ . Therefore, we only need to derive the  $tt$  and  $rt$  components of  $\mathbb{W}_{0\nu}$ , whereas the  $tr$  and  $rr$  components are irrelevant. It turns out that this also holds for the inner terms of the recursion (4.100): we only need the  $tt$  and  $rt$  components of the intermediate  $\mathbb{W}_{0a}$ .

## 5 Evanescent waves

{Seva}

### 5.1 Vanishing vertical wavenumber, evanescent case etc

Fragments from different sources...

#### 5.1.1 Vanishing vertical wavenumber

{Snokz}

The general solution of (2.10) will be a linear function of  $z$ :

$$\phi_l(z) = A_l^0 + A_l^1 z. \quad (5.1) \quad \{\{Ephilz\}\}$$

In BornAgain, such a linear wavefunction amplitude can not be handled by the form factors, which are only defined in terms of plane waves with complex wavevector components. The following cases are treated separately:

- There is only one layer: this is a trivial case without any need to calculate wave coefficients. The solution in the single layer is just the incoming/outgoing plane wave.
- The top layer of a multilayer has  $\kappa_0 = 0$ : the limit  $\kappa_0 \rightarrow 0$  is well-defined and the solution is given by  $A_0^+ = -A_0^-$  and  $A_l^\pm = 0$  for  $l > 0$ .
- $\kappa_l = 0$  for a layer with  $l > 0$ : In this case  $\kappa_l$  will be given a very small imaginary value, representing a slight absorption. However, this should be inconsequential because the index of refraction of non-vacuum layer always contains an absorptive component.

#### 5.1.2 Opaque layers and evanescent waves

{Sevawa}

TODO: Rework this fragment (ingested 29may23 from ba-intern/theory/Stratified.tex).

For incident angles below the critical angle  $\alpha_i < \alpha_c$  (also at interfaces inside the sample), the  $k_z$ -component of the wave vector turns imaginary. This situation then corresponds to an evanescent wave. As a consequence, the phase factor  $\delta$  (2.29) turns real and describes the exponential decrease of the amplitudes  $t_j, r_j$  in the corresponding layer. For large layer thicknesses, this means that  $\delta$  rapidly approaches zero, and its inverse becomes very large. This leads to an increasingly ill-conditioned transfer matrix ??, until, at some point, both quantities underflow or overflow, leading to invalid numerical results.

As the simulation approaches this singular situation, the amplitudes  $t_j$  and  $r_j$  will rapidly increase towards the top of a sample and potentially overflow at some point before the computation reaches the top layer. Intuitively, this can easily be understood as follows. As we impose the boundary condition  $t_\nu = 1$ ,  $r_\nu = 0$  in the substrate for incident angles below the critical angle with  $T = 0$ ,  $R = 1$ , this means, that we must find  $t_0 \rightarrow \infty$ . Obviously, this cannot be implemented numerically in a sane manner.

In order to detect and handle this over/underflow, BornAgain checks for an overflow of  $t_j$ .

It must be mentioned though, that this algorithm still fails if a very thick layer is encountered. This will lead to the immediate underflow of  $\delta$  and hence to an overflow of  $\delta^{-1}$ . This means, that the transmission of a single layer is within the numerical precision zero, but the mathematical formulation applied cannot handle this corner case and the computation still crashes. Therefore, the only way to circumvent this problem is by restarting the computation from the current layer by reapplying the boundary condition  $t_j = 1$ ,  $r_j = 0$  and setting all amplitudes in the layers below to zero.

### 5.1.3 Flux, evanescent waves

{SSpecial}

We write

$$\kappa =: \kappa' + i\kappa'' \quad (5.2) \quad \{\text{Edecompkperp}\}$$

for the decomposition into a real and an imaginary part. Accordingly, full wavevectors have the decomposition

$$\mathbf{k}^\pm =: \mathbf{k}^{\pm'} + i\mathbf{k}^{\pm''} = \mathbf{k}_\parallel \pm (\kappa' + i\kappa'')\hat{\mathbf{z}}. \quad (5.3) \quad \{\text{Edecompkperp}\}$$

Per (1.30), we have  $\beta \geq 0$  and  $\delta < 1$ , from which it follows that  $\kappa''$  always has the same sign as  $\kappa'$ .

After these preparations, we can compute the flux (1.9):

$$\begin{aligned} \mathbf{J}(\mathbf{r}) = & |A^-|^2 e^{+2\kappa''(z-z_l)} \mathbf{k}^{-'} + |A^+|^2 e^{-2\kappa''(z-z_l)} \mathbf{k}^{+'} \\ & + \left[ A^- A^{+*} e^{-2i\kappa'(z-z_l)} (\mathbf{k}_\parallel - i\kappa''\hat{\mathbf{z}}) + \text{c.c.} \right]. \end{aligned} \quad (5.4) \quad \{\text{EJ1}\}$$

The first two terms describe the exponential intensity decrease due to absorption, while the oscillatory term in square brackets is responsible for waveguide effects in layers with finite thickness. The flux can also be written in terms of the one-dimensional wavefunctions  $\phi^\pm(z)$ :

$$\begin{aligned} \mathbf{J}(\mathbf{r}) = & |\phi^+(z) + \phi^-(z)|^2 \cdot \mathbf{k}_\parallel \\ & + \left[ |\phi^+(z)|^2 \kappa' - |\phi^-(z)|^2 \kappa' + 2 \text{Im}(\phi^-(z)\phi^{+*}(z))\kappa'' \right] \cdot \hat{\mathbf{z}}. \end{aligned} \quad (5.5) \quad \{\text{EJ2}\}$$

The first term denotes the horizontal component of the flux and can be seen to consist of the product of the particle density at position  $z$  and the wavevector  $\mathbf{k}_\parallel$ . The  $z$ -component consists of the difference between the up- and downward travelling wave components and an extra term that encodes the interference between them.

In the special case of a purely imaginary  $\kappa_l$ , the flux becomes:

$$\mathbf{J}(\mathbf{r}) = |\psi|^2 \mathbf{k}_{\parallel} + 2 \operatorname{Im}(A^- A^{+*}) \kappa'' \hat{\mathbf{z}}. \quad (5.6) \quad \{\text{EJ3}\}$$

This flux consists of two clearly distinct parts: an *evanescent wave*, travelling horizontally and a vertical component that is independent of the  $z$  position. The vertical component is a necessary degree of freedom to fulfill the boundary conditions at the layer's top and bottom interfaces. In the case of a semi-infinite layer, the vertical component becomes zero and all incoming radiation at the top of the layer undergoes *total reflection*.

# 6 Instrument simulation

## 6.1 Incoming beam and resolution

{SInstr}

{SBeam}

to be written ...



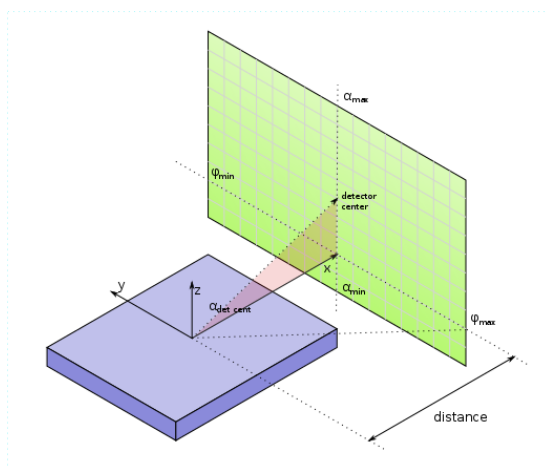


Figure 6.1: Experimental geometry with a two-dimensional pixel detector.

{FexpGeom}

## 6.2 Detector images

{SdetImg}

To conclude this chapter on the foundations of small-angle scattering, we shall derive the geometric factors that allow us to convert differential cross sections into detector counts. We shall also discuss how to present data on a physically meaningful scale.

### 6.2.1 Pixel coordinates, scattering angles, and $\mathbf{q}$ components

We assume that scattered radiation is detected in a flat, two-dimensional detector that generates histograms on a rectangular grid, consisting of  $n \cdot m$  pixels of constant width and height, as sketched in Fig. 6.1. This figure also shows the coordinate system according to unanimous GISAS convention, with  $z$  normal to the sample plane, and with the incident beam in the  $xz$  plane. The origin is at the center of the sample surface. We suppose that the detector is mounted perpendicular to the  $x$  axis at a distance  $L$  from the sample position. The real-space coordinate at the center of pixel  $(i, j)$  is  $(L, y_i, z_i)$ . Each pixel has a width  $\Delta y$  and a height  $\Delta z$ . BornAgain requires a full parametrization of the detector geometry to correctly perform the affine-linear mapping from pixel indices  $i, j$  to pixel coordinates  $x_i, y_i$ ; see the [rectangular detector tutorial](#).

Since the differential scattering cross section (1.31) is given with respect to a solid-angle element  $d\Omega$ , we need to express the scattered wavevector  $\mathbf{k}_f$  in spherical coordinates, using the horizontal azimuth angle  $\phi_f$  and the vertical glancing angle  $\alpha_f$ . The projection of  $(\alpha_f, \phi_f)$  into the detector plane  $(y, z)$  is known as the *gnomonic projection*. From elementary trigonometry one finds

$$\begin{aligned} y &= L \tan \phi_f, \\ z &= (L / \cos \phi_f) \tan \alpha_f. \end{aligned} \tag{6.1} \quad \{\text{Eyzdet}\}$$

Fig. 6.2 shows lines of equal  $\alpha_f, \phi_f$  in the detector plane. To emphasize the curvature of the constant- $\alpha_f$  lines, scattering angles up to more than  $25^\circ$  are shown. In typical SAS

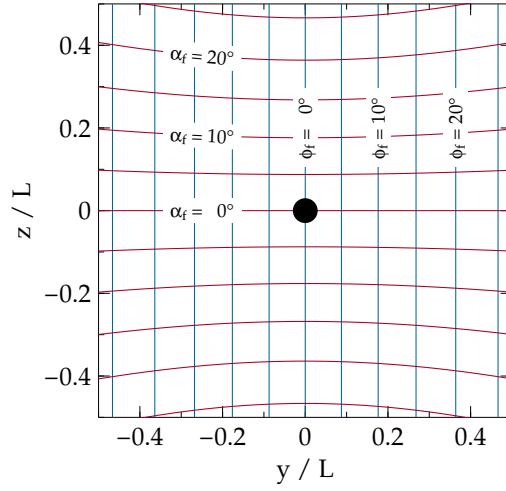


Figure 6.2: Lines of constant  $\alpha_f$  (red) or  $\phi_f$  (blue) in the detector plane, for a planar detector at distance  $L$  from the sample. The black dot indicates the beamstop location for the central incident beam (SAS geometry,  $\hat{\mathbf{k}}_i = \hat{x}$ ).

$\{\text{Fconstalphi}\}$

or GISAS, scattering angles are much smaller, and therefore the mapping between pixel coordinates and scattering angles is in a good first approximation linear. Of course BornAgain is not restricted to this linear regime, but uses the exact nonlinear mapping (6.1).

To determine the scattering vector  $\mathbf{q}_{ij}$  that corresponds to a pixel  $(i, j)$ , we need to express the outgoing wavevector  $\mathbf{k}_f$  as function of  $y$  and  $z$ . This can be done either by inverting (6.1) and inserting the so obtained  $\alpha_f(y, z)$  and  $\phi_f(y)$  in

$$\mathbf{k}_f = K \begin{pmatrix} \cos \alpha_f \cos \phi_f \\ \cos \alpha_f \sin \phi_f \\ \sin \alpha_f \end{pmatrix}, \quad (6.2) \quad \{\{\text{Ekf\_by\_angle}\}\}$$

or much more directly by using geometric similarity in Cartesian coordinates. The result is rather simple:

$$\mathbf{k}_f = \frac{K}{\sqrt{L^2 + y^2 + z^2}} \begin{pmatrix} L \\ y \\ z \end{pmatrix}. \quad (6.3) \quad \{\{\text{Ekf\_by\_pixel}\}\}$$

The transform (6.6) between pixel coordinates  $y, z$  and physical scattering vector components  $q_y, q_z$  is nonlinear, due to the square-root term in the denominator of (6.3). For  $y, z \ll L$ , however, nonlinear terms loose importance.

The left detector frame in Fig. 6.3 shows circles of constant values of  $\pm q_x$ . For given steps in  $q_x$ , the distance between adjacent circles increases towards the detector center. From ?? and (6.3), one finds asymptotically for  $y, z \rightarrow L$  that  $q_x$  goes with the



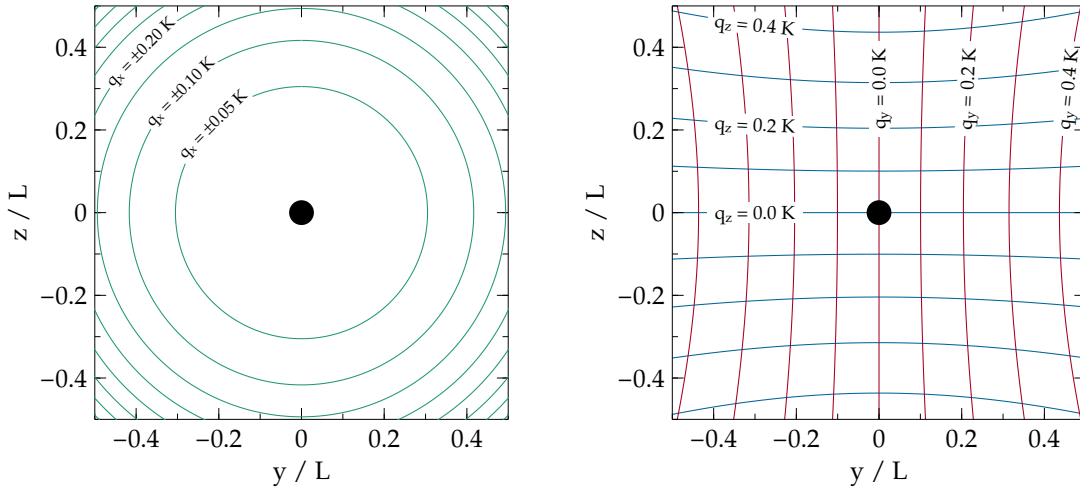


Figure 6.3: Lines of constant  $q_x$  (left),  $q_y$  or  $q_z$  (right), in units of the incident wavenumber  $K = 2\pi/\lambda$ , for a planar detector. SAS geometry as in Fig. 6.2.

{Fconstq}

square of the two other components of the scattering vector,

$$\frac{q_x}{K} \doteq \frac{y^2 + z^2}{2L^2} \doteq \frac{q_y^2 + q_z^2}{2K^2}. \quad (6.4) \quad \{\{Eqxasy\}\}$$

Therefore, under typical small angle conditions  $y, z \rightarrow L$  the dependence of the scattering signal on  $q_x$  is unimportant: one basically measures  $v(\mathbf{q}) \simeq v(0, q_y, q_z)$ . The exception, for sample structures with long correlations in  $x$  direction, is illustrated in Fig. 6.4.

As anticipated in (6.4), the other two components of  $\mathbf{q}$  are in first order linear in the pixel coordinates,

$$\frac{q_y}{K} = \frac{y}{L} \left( 1 - \frac{y^2 + z^2}{2L^2} + \dots \right), \quad (6.5) \quad \{\{Eqxasy\}\}$$

and similarly for  $q_z$ . The nonlinear correction terms lead to the pincushion distortion shown in the right detector frame in Fig. 6.3.

Since pixel coordinates are meaningful only with respect to a specific experimental setup, users may wish to transform detector images towards the physical coordinates  $q_y$  and  $q_z$ . As shown in Fig. 6.5, this would yield a barrel-shaped illuminated area in the  $q_y, q_z$  plane.

To summarize this section, the wavevector  $\mathbf{q}_{ij}$  can be determined from the pixel

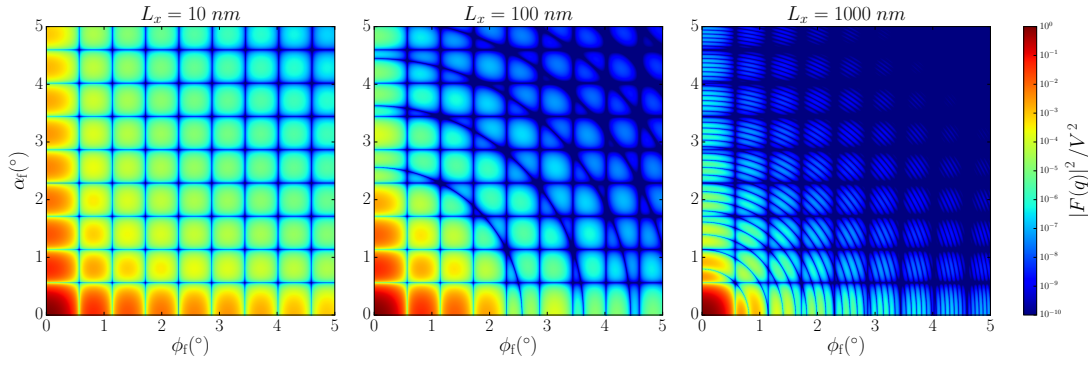


Figure 6.4: Simulated detector image for small-angle scattering from uncorrelated cuboids (right rectangular prisms). The incoming wavelength is 0.1 nm. The prisms have edge lengths  $L_y = L_z = 10$  nm; the length  $L_x$ , in beam direction, is varied as shown above the plots. The circular modulation comes from a factor  $\text{sinc}(q_x L_x/2)$  in the cuboid form factor, with  $q_x$  given by (6.4).

{Fdetbox}

indices through the following steps:

$$\begin{aligned}
 &(i, j) \\
 &\quad \downarrow \quad \text{calibrate of origin, then employ affine-linear mapping} \\
 &(y, z) \\
 &\quad \downarrow \quad \text{use (6.3)} \\
 &\mathbf{k}_f \\
 &\quad \downarrow \quad \text{use (??)} \\
 &\mathbf{q}
 \end{aligned} \tag{6.6} \quad \{\{E\text{qalgo}\}\}$$

Transforming detector images from pixel coordinates into the  $q_y, q_z$  plane is not implemented in BornAgain, and not on our agenda. We would, however, like to hear about use cases.

When simulating and fitting experimental data with BornAgain, detector images remain unchanged. All work is done in terms of reduced pixel coordinates  $y/L$  and  $z/L$ . Corrections are applied to the simulated, not to the measured data.

...show how to plot  $q$  grid on top of detector image ...

## 6.2.2 Intensity transformation

The solid angle under which a detector pixel is illuminated from the sample is in linear approximation

$$\Delta\Omega = \cos\alpha_f \Delta\alpha_f \Delta\phi_f = \cos\alpha_f \left| \frac{\partial(\alpha_f, \phi_f)}{\partial(y, z)} \right| \Delta y \Delta z = \cos^3\alpha_f \cos^3\phi_f \frac{\Delta y \Delta z}{L^2}. \tag{6.7} \quad \{\{E\text{qalgo}\}\}$$

Altogether, the expected count rate in detector pixel  $(i, j)$  is proportional to

$$I_{ij} = \cos^3\alpha_f \cos^3\phi_f \frac{d\sigma}{d\Omega}(\mathbf{q}_{ij}), \tag{6.8} \quad \{\{E\text{Itrafo\_cos}\}\}$$

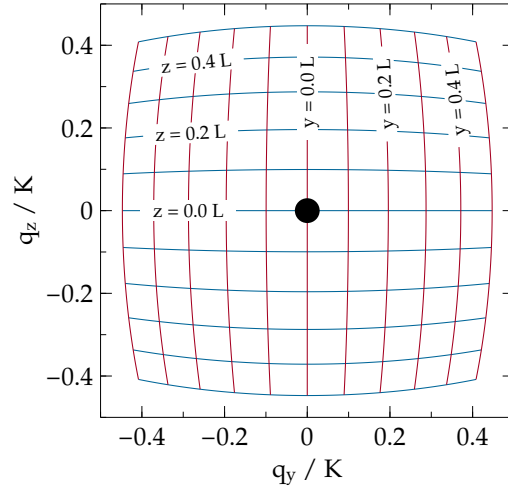


Figure 6.5: The outer contour of the blue and red grid shows the border of a square detector image after transformation into the physical coordinates  $q_y$ ,  $q_z$ . The blue and red curves correspond to horizontal and vertical lines in the detector.

{Fconstp}

where we have omitted constant factors  $L^{-2}$ ,  $\Delta y$  and  $\Delta z$ . Using pixel coordinates instead of angles, this can be rewritten as

$$I_{ij} = \left(1 + \frac{y^2 + z^2}{L^2}\right)^{-3/2} \frac{d\sigma}{d\Omega}(\mathbf{q}_{ij}(y, z)). \quad (6.9) \quad \{\{E\text{Itrafo\_pix}\}\}$$

# Bibliography

- [1] G. Pospelov, W. Van Herck, J. Burle, J. M. Carmona Loaiza, C. Durniak, J. M. Fisher, M. Ganeva, D. Yurov and J. Wuttke, *J. Appl. Cryst.* **53**, 262 (2020). [ii](#), [1:1](#), [1:4](#), [3:11](#)
- [2] V. P. Sears, *Neutron News* **3**, 26 (1992). [1:2](#)
- [3] V. P. Sears, *Neutron Optics*, Oxford University Press: Oxford (1989). [1:2](#)
- [4] G. Renaud, R. Lazzari and F. Leroy, *Surf. Sci. Rep.* **64**, 255 (2009). [1:3](#)
- [5] M. v. Laue, *Erg. exakt Naturwiss.* **10**, 133 (1931). [1:3](#)
- [6] G. H. Vineyard, *Phys. Rev. B* **26**, 4146 (1982). [1:5](#)
- [7] P. Mazur and D. L. Mills, *Phys. Rev. B* **26**, 5175 (1982). [1:5](#)
- [8] S. Dietrich and H. Wagner, *Z. Phys. B* **56**, 207 (1984). [1:5](#)
- [9] S. Dietrich and H. Wagner, *Z. Phys. B* **59**, 35 (1985). [1:5](#)
- [10] H. Schober, *J. Neutron Res.* **17**, 109 (2014). [1:6](#)
- [11] F. Abelès, *J. Phys. Radium* **11**, 307 (1950). [2:6](#)
- [12] J. D. Jackson, *Classical Electrodynamics*, John Wiley: New York (<sup>2</sup>1975). [2:7](#)
- [13] G. Kohn, V. J. Moscow Phys. Soc. **1**, 425 (1991). [2:9](#), [4:17](#)
- [14] S. A. Stepanov, E. A. Kondrashkina, R. Köhler, D. V. Novikov, G. Materlik and S. M. Durbin, *Phys. Rev. B* **57**, 4829 (1998). [2:9](#), [2:10](#), [4:17](#)
- [15] L. G. Parratt, *Phys. Rev.* **95**, 359 (1954). [2:10](#)
- [16] J. Lekner, *Theory of Reflection*, Springer: Cham (<sup>2</sup>2016). [3:1](#), [3:2](#)
- [17] L. D. Landau and E. M. Lifschitz, *Lehrbuch der theoretischen Physik, III. Quantenmechanik*, Akademie-Verlag: Berlin (<sup>7</sup>1985). [3:1](#), [4:2](#)
- [18] A. V. Andreev, A. G. Michette and A. Renwick, *J. Mod. Opt.* **35**, 1667 (1988). [3:2](#)

- [19] M. Tolan, *X-ray scattering from soft-matter thin films. Materials science and basic research* (Springer Tracts in Modern Physics 148), Springer: Berlin (1999). 3:3, 3:15
- [20] D. K. G. de Boer and A. J. G. Leenaers, *Physica B* **221**, 18 (1996). 3:3, 3:14
- [21] L. Névot, B. Pardo and J. Corno, *Rev. Phys. Appl.* **23**, 1675 (1988). 3:3
- [22] A. Gibaud and G. Vignaud, in *X-ray and Neutron Reflectivity*, edited by J. Dailant and A. Gibaud (Lect. Notes Phys. 770) (2009). 3:3
- [23] S. K. Sinha, E. B. Sirota, S. Garoff and H. B. Stanley, *Phys. Rev. B* **38**, 2297 (1988). 3:5, 3:10, 3:12, 3:13, 3:15
- [24] V. Holý, J. Kubena, I. Ohlídal, K. Lischka and W. Plotz, *Phys. Rev. B* **47**, 15896 (1993). 3:5, 3:10, 3:13
- [25] E. W. Weisstein, *Bivariate Normal Distribution*. <https://mathworld.wolfram.com/BivariateNormalDistribution.html>. 3:9
- [26] B. Pynn, *Phys. Rev. B* **45**, 602 (1992). 3:10, 3:13
- [27] L. Névot and P. Croce, *Rev. Phys. Appl.* **15**, 761 (1980). 3:10, 3:11, 3:13
- [28] M. Abramowitz and I. Stegun, *Handbook of Mathematical Functions*, National Bureau of Standards (1964). 3:11
- [29] J.-P. Schlomka, M. Tolan, L. Schwalowsky, O. H. Seeck, J. Stettner and W. Press, *Phys. Rev. B* **51**, 2311 (1995). 3:11, 3:12
- [30] A. Steyerl, *Z. Phys.* **254**, 169 (1972). 3:13
- [31] Y. A. Baloshin and A. V. Kostin, *Optics Commun.* **160**, 22 (1999). 3:13
- [32] A. Steyerl, S. S. Malik and L. R. Iyengar, *Physica B* **173**, 47 (1991). 3:13
- [33] P. Beckmann and A. Spizzichino, *The Scattering of Electromagnetic Waves from Rough Surfaces*, Artech House: Norwood, MA (1987). 3:13
- [34] V. Holý and T. Baumbach, *Phys. Rev. B* **49**, 10668 (1994). 3:14
- [35] U. Pietsch, V. Holý and T. Baumbach, *High-Resolution X-Ray Scattering*, Springer: New York (2004). 3:14
- [36] D. K. G. de Boer, *Phys. Rev. B* **49**, 5817 (1994). 3:14, 3:15, 3:16
- [37] D. K. G. de Boer, *Phys. Rev. B* **53**, 6048 (1996). 3:14, 3:15, 3:16
- [38] D. K. G. de Boer, *Phys. Rev. B* **44**, 498 (1991). 3:14
- [39] D. K. G. de Boer, *Phys. Rev. B* **51**, 5297 (1995). 3:14, 3:15
- [40] A. Caticha, *Phys. Rev. B* **52**, 9214 (1995). 3:15

- [41] M. Rauscher, T. Salditt and H. Spohn, Phys. Rev. B **52**, 16855 (1995). 3:15
- [42] S. Dietrich and A. Haase, Phys. Rev. **260**, 1 (1995). 3:15
- [43] H. Ogura and N. Takahashi, Progress in Electromagnetic Research PIER **14**, 89 (1996). 3:15
- [44] B. P. Toperverg, O. Schärpf and I. S. Anderson, Physica B **276–278**, 954 (2000). 3:15
- [45] Y. Fujii, IOP Conf. Series: Mat. Sci. and Eng. **42**, 012009 (2011). 3:15
- [46] Y. Fujii, Acta Cryst. A **56** (2013). 3:15
- [47] Y. Fujii, Japan. J. Appl. Phys. **53**, 05FH06 (2014). 3:15
- [48] Y. Fujii, T. MRS Jap. **40**, 369 (2015). 3:15
- [49] F. N. Chukhovskii, Acta Cryst. A **67**, 200 (2011). 3:16
- [50] F. N. Chukhovskii, Acta Cryst. A **68**, 505 (2012). 3:16
- [51] F. N. Chukhovskii and B. S. Roshchin, Acta Cryst. A **71**, 612 (2015). 3:16
- [52] R. Maruyama, D. Yamazaki and K. Soyama, J. Phys. Soc. Jpn. **22** (2018). 3:16
- [53] A. Hafner, PhD thesis, University Libre de Bruxelles, Institutue Laue-Langevin (2019). 3:16
- [54] H. Zabel, K. Theis-Bröhl and B. P. Toperverg, in *Handbook of Magnetism and Advanced Magnetic Materials. Volume 3: Novel Techniques for Characterizing and Preparing Samples*, edited by H. Kronmüller and S. Parkin, John Wiley (2007). 4:1
- [55] E. Kentzinger, U. Rücker and B. Toperverg, Physica B **335**, 82 (2003). 4:2, 4:7, 4:16
- [56] E. Kentzinger, U. Rücker, B. Toperverg, F. Ott and T. Brückel, Phys. Rev. B **77**, 104435 (2008). 4:2, 4:7
- [57] C. F. Majkrzak, K. V. O'Donovan and N. F. Berk, in *Neutron Scattering from Magnetic Materials*, edited by T. Chatterji, Elsevier: Amsterdam (2006). 4:12
- [58] B. P. Toperverg, Phys. Met. Metallogr. **116**, 1337 (2015). 4:14
- [59] A. R. Wildes, Review of Scientific Instruments **70**, 4241 (1999). 4:14
- [60] A. R. Wildes, Neutron News **17**, 17 (2006). 4:14